Circular 1514

UF UNIVERSITY of FLORIDA
IFAS Extension

Field Observations During the Fifth Microwave Water and Energy Balance Experiment (MicroWEX-5): from March 9 through May 26, 2006[1]

Joaquin Casanova, Fei Yan, Mi-young Jang, Juan Fernandez, Jasmeet Judge, Clint Slatton, Kai-Jen Calvin Tien, Tzu-yun Lin, Orlando Lanni, and Larry Miller[2]

1. This document is Circular 1514, one of a series of the Agricultural and Biological Engineering Department, Florida Cooperative Extension Service, Institute of Food and Agricultural Sciences, University of Florida. First published May 2007. Reviewed March 2020. Please visit the EDIS Website at https://edis.ifas.ufl.edu for more publications.

This research was supported by funding obtained from the NASA-NIP Grant #00050655 and NSF Earth Science Directorate (EAR-0337277).

2. Joaquin Casanova, Fei Yan, Mi-young Jang, and Juan Fernandez are graduate research assistants at the University of Florida (UF); Jasmeet Judge is an Assistant Professor and Director of Center for Remote Sensing of UF (email: jasmeet@ufl.edu); Clint Slatton is an Assistant Professor of UF; Kai-Jen Tien, and Tzu-Yun Lin are graduate research assistants at UF; and Orlando Lanni and Larry Miller are Engineers of UF. All authors except Juan Fernandez and Clint Slatton affiliated with the Agricultural and Biological Engineering Department, Institute of Food and Agricultural Sciences, University of Florida, Gainesville, FL 32611. Juan Fernandez and Clint Slatton are with Geosensing Systems Engineering, Department of Civil & Coastal Engineering, University of Florida, Gainesville, FL 32611

Reviewed: 12/2024

TABLE OF CONTENTS

1. INTRODUCTION **1**

2. OBJECTIVES **1**

3. FIELD SETUP **1**

4. SENSORS **3**

4.1 University of Florida Microwave Radiometer Systems **4**

4.1.1 University of Florida C-band Microwave Radiometer (UFCMR) **4**

4.1.1.1 Theory of operation **5**

4.1.2 University of Florida L-band Microwave Radiometer (UFLMR) **7**

4.1.2.1 Theory of operation **9**

4.2 Eddy Covariance System **11**

4.3 Net Radiometer **12**

4.4 Precipitation measurement **12**

4.5 Air Temperature and Relative Humidity **12**

4.6 Canopy Air Temperature **13**

4.7 Soil Moisture and Temperature Probe **14**

4.8 Soil Heat Flux Plate **14**

5. SOIL SAMPLING **14**

5.1 Soil Surface Roughness **14**

6. VEGETATION SAMPLING **15**

6.1 Heightand Width **15**

6.2 Leaf Area Index (LAI) **15**

6.3 Green and Dry Biomass **15**

6.4 Vertical Distribution of Moisture in the Canopy **15**

7. WELL SAMPLING **16**

7.1 Groundwater sampling **16**

7.2 Water level measurement **16**

8. FIELD LOG **16**

9. REFERENCES **20**

10. ACKNOWLEDGMENTS **21**

A. FIELD OBSERVATIONS **22**

1. INTRODUCTION

For accurate prediction of weather and near-term climate, root-zone soil moisture is one of the most crucial components driving the surface hydrological processes. Soil moisture in the top meter is also very important because it governs moisture and energy fluxes at the land-atmosphere interface and it plays a significant role in partitioning of the precipitation into runoff and infiltration.

Energy and moisture fluxes at the land surface can be estimated by Soil-Vegetation-Atmosphere-Transfer (SVAT) models. These models are typically used in conjunction with climate prediction models and hydrological models. Even though the biophysics of moisture and energy transport is well-captured in most current SVAT models, the computational errors accumulate over time and the model estimates of soil moisture diverge from reality. One promising way to significantly improve model estimates of soil moisture is by assimilating remotely sensed data that are sensitive to soil moisture, for example microwave brightness temperatures, and updating the model state variables.

The microwave brightness at low frequencies (< 10 GHz) is very sensitive to soil moisture in the top few centimeters in most vegetated surfaces. Many studies have been conducted in agricultural areas such as bare soil, grass, soybean, wheat, pasture, and corn to understand the relationship between soil moisture and microwave remote sensing. Most of these experiments conducted in agricultural regions have been short-term experiments that captured only a part of growing seasons. It is important to know how microwave brightness signature varies with soil moisture, evapotranspiration (ET), and biomass in a dynamic agricultural canopy with a significant biomass (4-6 kg/m^2) throughout the growing season.

2. OBJECTIVES

The goal of MicroWEX-5 was to understand the land-atmosphere interactions during the growing season of corn, and their effect on observed microwave brightness signatures at 6.7 GHz and 1.4 GHz, matching that of the satellite-based microwave radiometers, AMSR, and the SMOS mission, respectively. Specific objectives of MicroWEX-5 are:

1. To collect passive microwave and other ancillary data to develop and calibrate a dynamic microwave brightness model for corn
2. To collect energy and moisture flux data at land surface and in soil to develop and calibrate a dynamic SVAT model for corn
3. To evaluate feasibility of soil moisture retrievals using passive microwave data at 6.7 and 1.4 GHz for the growing corn canopy

3. FIELD SETUP

MicroWEX-5 was conducted by the Center for Remote Sensing, Agricultural and Biological Engineering Department at the Plant Science Research and Education Unit (PSREU), IFAS, Citra, FL. Figure 1 and 2 show the location of the PSREU and the study site for the MicroWEX-5, respectively. The study site was located at the west side of the PSERU. The dimensions of the study site were a 183 m X 183 m. A linear move system was used for irrigation. The corn was planted on March 9 (Day of Year (DoY) 68) in 2006, at an orientation 60º from East as shown in Figure 3. The crop spacing was about 8 cm and the row spacing was 76.2 cm (30 inches). Instrument installation began on March 10 (DoY 69). The instruments consisted of a ground-based microwave radiometer system and micrometeorological stations. The ground-based microwave radiometer system was installed at the location shown in Figure 3, facing south to avoid the radiometer shadow interfering with the field of view as seen in Figure 3.

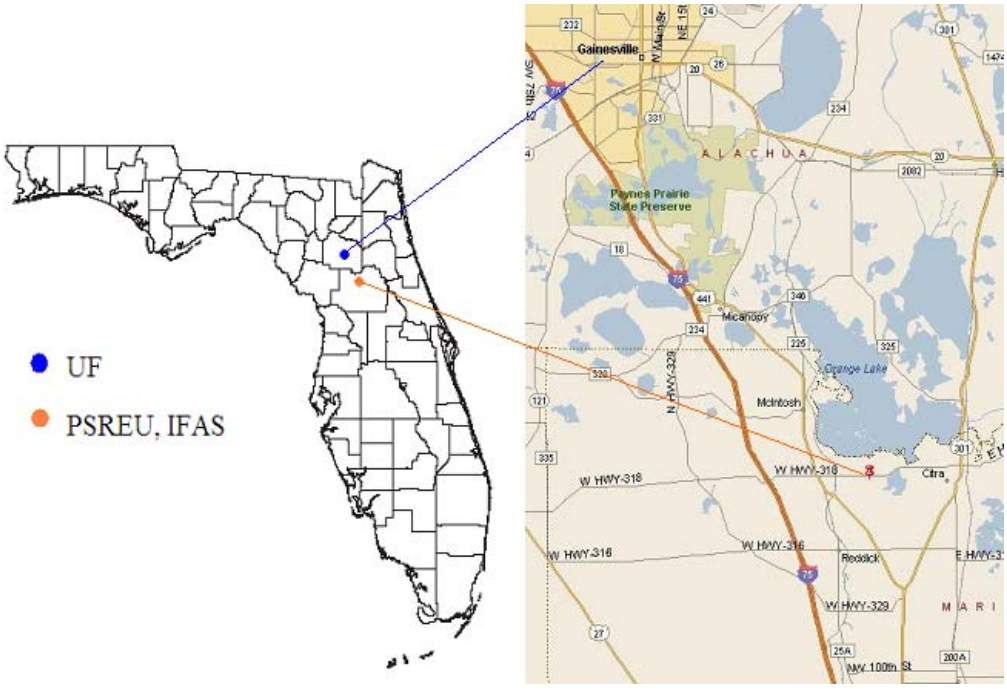

Figure 1. Location of PSREU/IFAS (from http://plantscienceunit.ifas.ufl.edu/directions.htm)

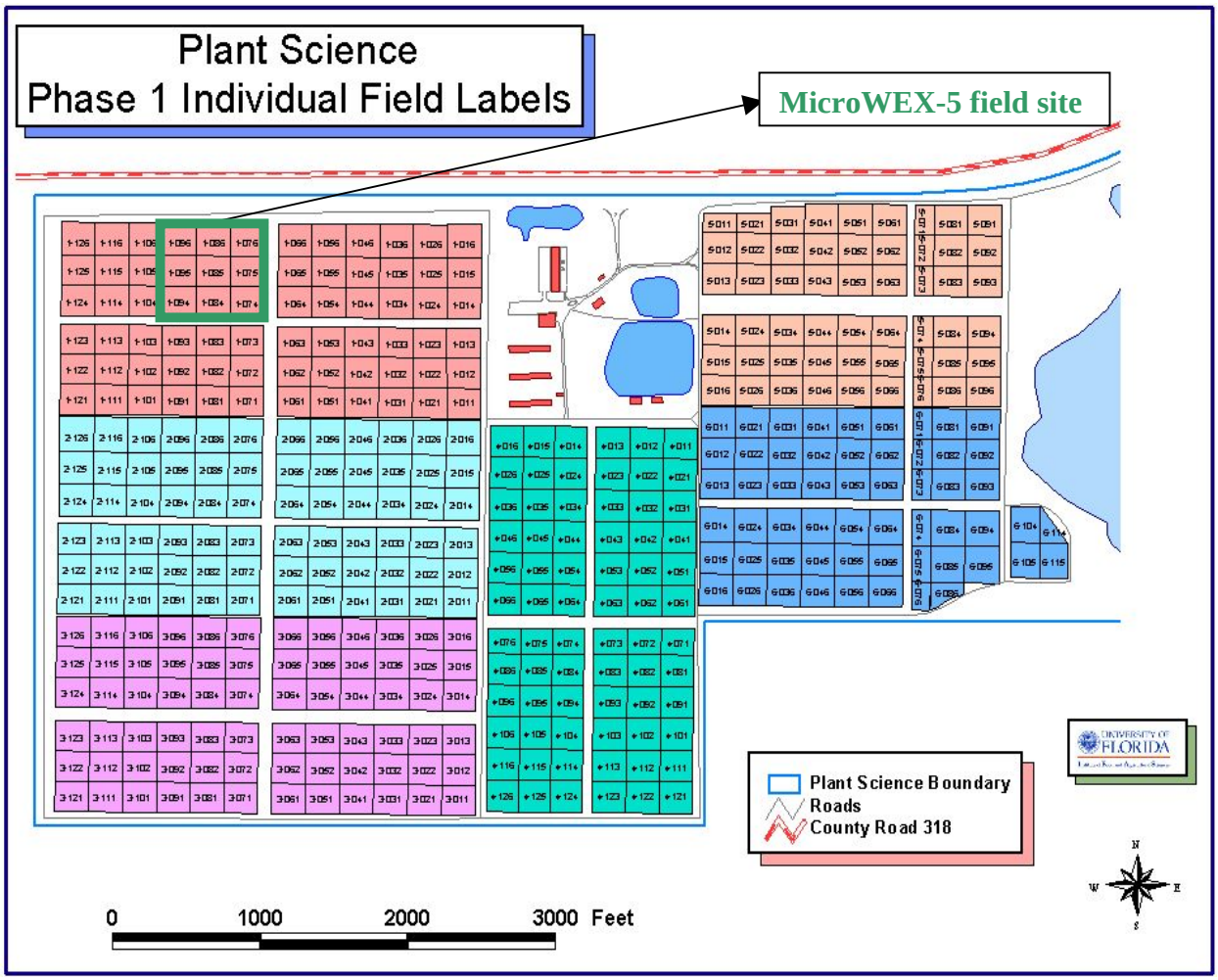

Figure 2. Location of the field site for MicroWEX-5 at the UF/IFAS PSREU (from http://plantscienceunit.ifas.ufl.edu/images/location/p1.jpg)

The micrometeorological station was installed at the center of the field and included soil heat flux plates and the eddy covariance system. Two raingauges were installed at the east and west edge of the radiometer footprints. Two additional raingauges also were installed at the east and west edge of the field to capture the irrigation. Three datalogging stations with soil moisture, soil heat flux, and soil temperature sensors installed were set up at the Northwest, East, and Southwest locations shown in Figure 3. A relative humidity (RH) sensor, temperature sensor, and net radiometer were installed at the Northwest station. This report provides detailed information regarding sensors deployed and data collected during the MicroWEX-5.

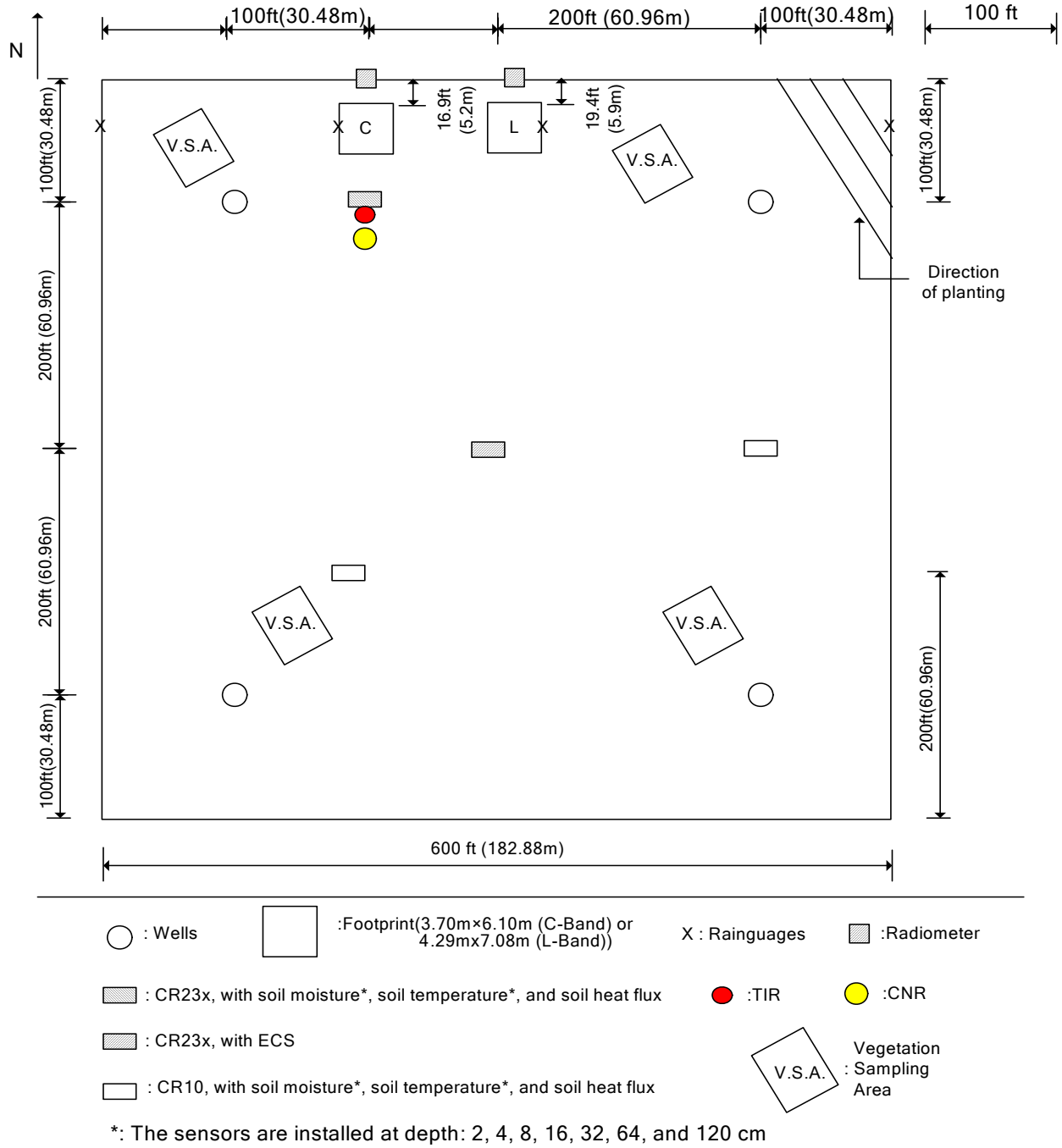

Figure 3. Layout of the sensors during MicroWEX-5.

4. SENSORS

MicroWEX-5 had three major types of instrument subsystems: the ground-based University of Florida C-band and L-band Radiometers, the micrometeorological subsystem, and the soil subsystem.

4.1 University of Florida Microwave Radiometer Systems

4.1.1 University of Florida C-band Microwave Radiometer (UFCMR)

Microwave brightness temperatures at 6.7GHz (λ = 4.48 cm) were measured every 15 minutes using the University of Florida's C-band Microwave Radiometer system (UFCMR) (Figure 4 (a)). The radiometer system consisted of a dual polarization total power radiometer operating at the center frequency of 6.7 GHz housed atop a 10 m tower installed on a 16' trailer bed. UFCMR was designed and built by the Microwave Geophysics Group at the University of Michigan. It operates at the center frequency at 6.7 GHz which is identical to one of the center frequencies on the space-borne Advanced Microwave Scanning Radiometer (AMSR) aboard the NASA Aqua Satellite Program. UFCMR observed the 3.70 m x 6.10 m footprint from a height of 5.90m. A rotary system was used to rotate the look angle of the UFCMR both for field observations and sky measurements. The brightness temperatures were observed at an incidence angle of 50˚. The radiometer was calibrated at least once every week with a microwave absorber as warm load and measurements of sky at several angles as cold load. Figure 4 (b) and 4 (c) show the close-up of the rotary system and the antenna of the UFCMR, respectively. Table 1 lists the specifications of UFCMR. Figure A-1 shows the V- & H-pol brightness temperatures observed during MicroWEX-5.

Table 1. UFCMR specifications

Parameter	**Qualifier**	**Value**
Frequency	Center	6.7 GHz
Bandwidth	3 dB	20 MHz
Beamwidth	3 dB V-pol elevation [a]	23°
	3 dB V-pol azimuth [b]	21°
	3 dB H-pol elevation [c]	21°
	3 dB H-pol azimuth [d]	23°
Isolation		> 27 dB
Polarizations	Sequential	V/H
Receiver temp		437 K
Noise Figure	From T_{rec}	3.99 dB
RF gain		85 dB
NEDT	1 sec	0.71 K
	8 sec	0.25 K

(a). sidelobes < -33 dB, (b). sidelobes < -28 dB, (c). sidelobes < -27 dB, (d). sidelobes < -35 dB

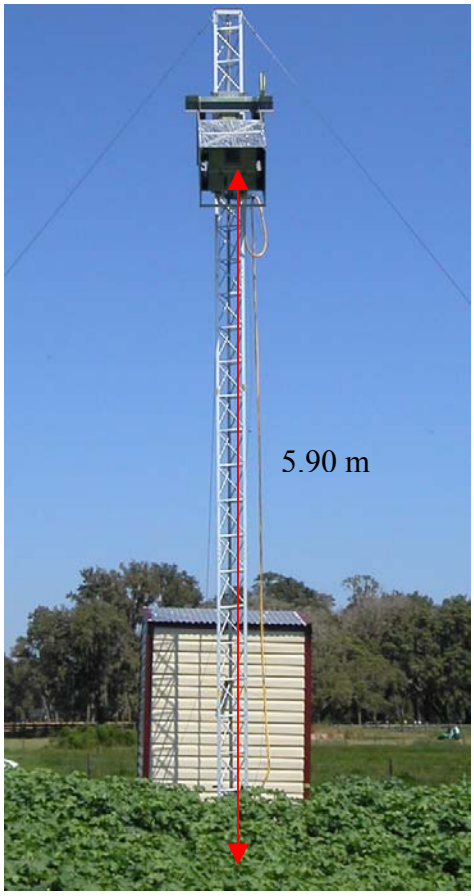

Figure 4 (a).The UFCMR system

Figure 4 (b) and (c). The side view of the UFCMR showing the rotary system and the front view of the UFCMR showing the receiver antenna.

4.1.1.1 Theory of operation

UFCMR uses a thermoelectric cooler (TEC) for thermal control of the Radio Frequency (RF) stages for the UFCMR. This is accomplished by the Oven Industries “McShane” thermal controller. McShane is used to cool or heat by Proportional-Integral-Derivative (PID) algorithm with a high degree of precision at 0.01°C. The aluminum plate to which all the RF components are attached is chosen to have sufficient thermal mass to eliminate short-term thermal drifts. All components attached to this thermal plate, including the TEC, use thermal paste to minimize thermal gradients across junctions.

The majority of the gain in the system is provided by a gain and filtering block designed by the University of Michigan for the STAR-Light instrument (De Roo, 2003). The main advantage of this gain block is the close proximity of all the amplifiers, simplifying the task of thermal control. This gain block was designed for a radiometer working at the radio astronomy window of 1400 to 1427 MHz, and so the receiver is a heterodyne type with downconversion from the C-band RF to L-band. To minimize the receiver noise figure, a C-band low-noise amplifier (LNA) is used just prior to downconversion. To protect the amplifier from saturation due to out of band interference, a relatively wide bandwidth, but low insertion loss, bandpass filter is used just prior to the amplifier. Between the filter and the antenna are three components: a switch for choosing polarization, a switch for monitoring a reference load, and an isolator to minimize changes in the apparent system gain due to differences in the reflections looking upstream from the LNA.

The electrical penetrations use commercially available weatherproof bulkhead connections (Deutsch connectors or equivalent). The heat sinks have been carefully located employing RTV (silicone sealant) to seal the bolt holes. The radome uses 15mil polycarbonate for radiometric signal penetration. It is sealed to the case using a rubber gasket held down to the case by a square retainer.

The first SMA connection is an electromechanical latching, which is driven by the Z-World control board switches between V- and H-polarization sequentially. The SMA second latching which switches between the analog signal from the first switch and the reference load signal from a reference load resistor sends the analog signal to a isolator, where the signal within 6.4 to 7.2 GHz in radiofrequency are isolated. Then the central frequency is picked up by a 6.7 GHz bandpass filter, which also protects the amplifier to saturation. A Low Noise Amplifier (LNA) is used to eliminate the noise figure and adjust gain. A mixer takes the input from the LNA and a local oscillator to output a 1.4 GHz signal to STAR-Lite. After the Power Amplifier and Filtering Block (Star-Lite back-end), the signal is passed through a Square Law Detector and a Post-Detection Amplifier (PDA). UFCMR is equipped with a microcontroller that has responsibility for taking measurements, monitoring the thermal environment, and storing data until a download is requested. A laptop computer is used for running the user interface named FluxMon to communicate with the radiometer through Radiometer Control Language (RadiCL). The radiometer is configured to maintain a particular thermal set point, and make periodic measurements of the brightness at both polarizations sequentially and the reference load. The data collected by the radiometer are not calibrated within the instrument, since calibration errors could corrupt an otherwise useful dataset. Figure 5 shows the block diagram of UFCMR.

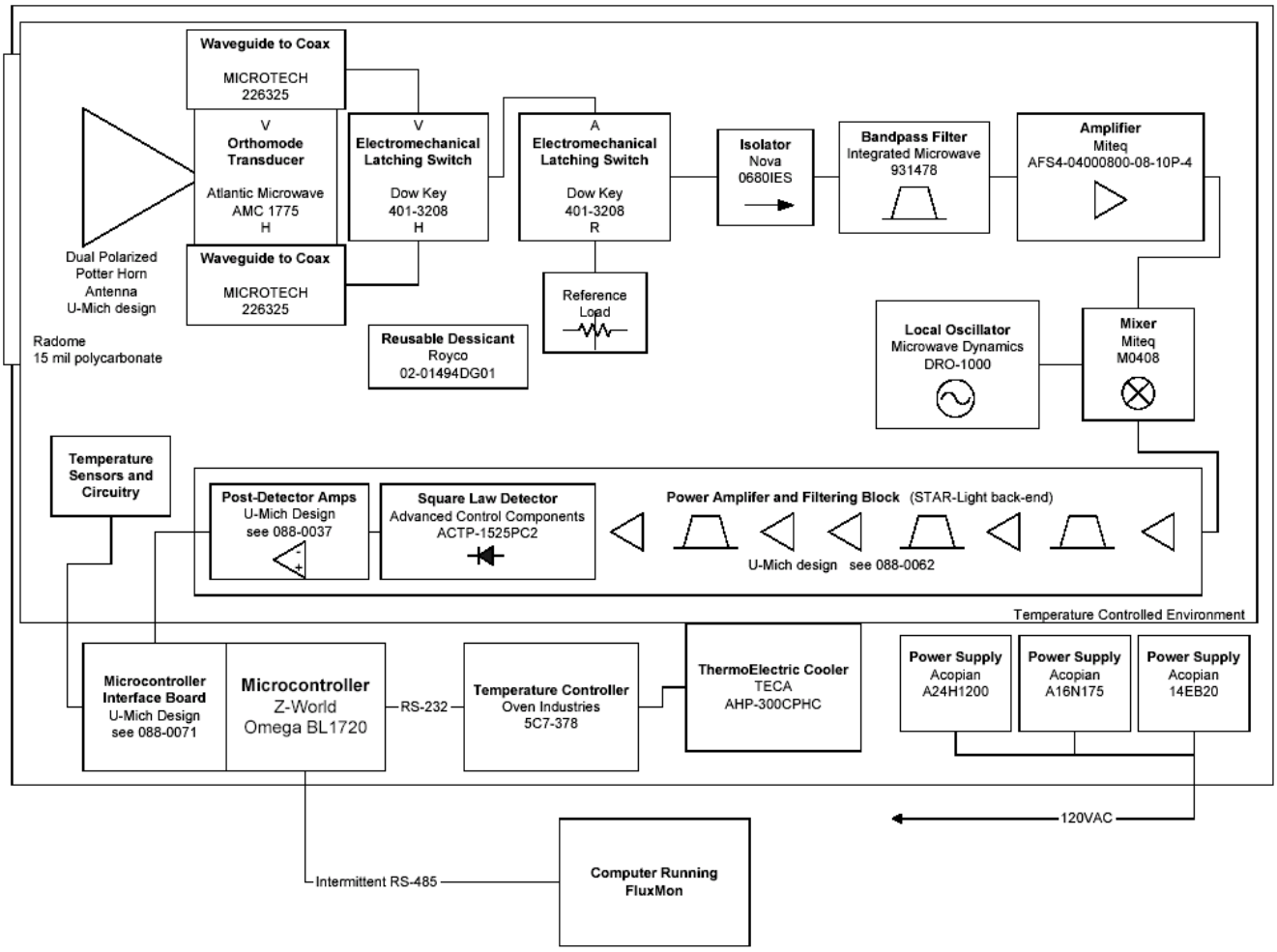

Figure 5. Block diagram of the University of Florida C-band Radiometer (De Roo, 2002).

4.1.2 University of Florida L-band Microwave Radiometer (UFLMR)

Microwave brightness temperature at 1.4GHz (λ = 21.0 cm) were measured every 15 minutes using the University of Florida's L-band Microwave Radiometer system (UFLMR) (Figure 6 (a)). The radiometer system consisted of a single polarization total power radiometer operating at the center frequency of 1.4 GHz housed atop a 9.14 m tower installed on a 16' trailer bed. UFLMR was designed and built by the Microwave Geophysics Group at the University of Michigan. It operates at the center frequency at 1.4 GHz which is identical to one of the center frequencies on the space borne Soil Moisture and Ocean Salinity (SMOS) mission. UFLMR observed the 4.29 m x 7.08 m footprint from a height of 6.81 m. A rotary system was used to rotate the look angle of the UFLMR both for field observations and sky measurements. The brightness temperatures were observed at an incidence angle of 50˚. The radiometer was calibrated at least every week with a microwave absorber as warm load and measurements of sky at several angles as cold load. Figure 6 (b) and 6 (c) show the close-up of the rotary system and the antenna of the UFLMR, respectively. Table 2 lists the specifications of UFLMR. Figure A-1 shows the H-pol brightness temperatures observed during MicroWEX-5.

Figure 6 (a).The UFLMR system

Figure 6 (b) and (c). The side view of the UFLMR showing the rotary system and the front view of the UFLMR showing the receiver antenna.

4.1.2.1 Theory of operation

UFLMR is similar to UFCMR in many respects, using a thermoelectric cooler (TEC) for thermal control, a similar electromechanical switching mechanism and a Z-World controller; the PDA is the same, and the software is a newer version of RadiCL. The RF block is designed for V- and H-pol switching, like the UFCMR, however, the UFLMR's septum horn antenna is single-polarized. As a result, only H-pol signal are guided from antenna to coax to the RF block, and the V-pol input to the RF block is an open circuit.

In the RF block, the first switch alternates between "V"- and H-pol and the second alternates between the reference load and the signal from the first switch. An isolator prevents reflections of the input signal. After the isolator, the signal goes through a bandpass filter and then an LNA, followed by a series of bandpass filters and Power Amplifiers before the Square Law Detector and the PDA. The microcontroller logs voltage and physical temperature measurements. Figure 7 shows the block diagram of UFLMR.

Table 2. UFLMR specifications

Parameter	**Qualifier**	**Value**
Frequency	Center	1.4 GHz
Bandwidth	3 dB	20 MHz
Beamwidth	3 dB H-pol elevation [a]	22.5°
	3 dB H-pol azimuth [b]	20.0°
Polarizations	Single	H
Receiver temp		179 K
Noise Figure	From T_{rec}	2.1 dB
RF gain		79 dB
NEDT		0.5 K

(a). sidelobes -20 dB, (b). sidelobes < -30 dB

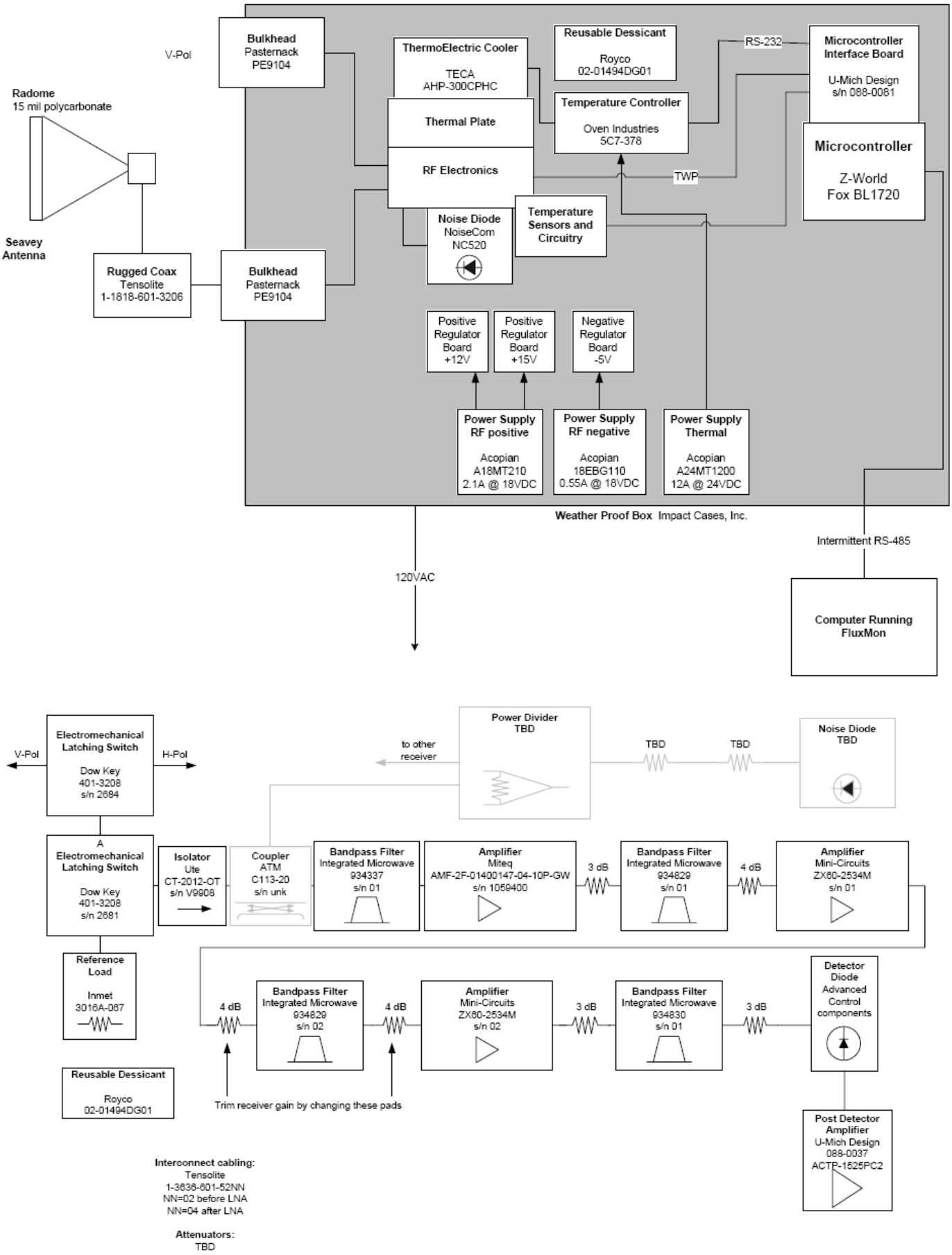

Figure 7. Block diagram of the University of Florida L-band Radiometer (De Roo, 2007).

4.2 Eddy Covariance System

A Campbell Scientific eddy covariance system was located at the center of the field also shown in Figure 8. The system included a CSAT3 anemometer and KH20 hygrometer. CSAT3 is a three dimensional sonic anemometer, which measures wind speed and the speed of sound on three non-orthogonal axes. Orthogonal wind speed and sonic temperature are computed from these measurements. KH20 measures the water vapor in the atmosphere. Its output voltage is proportional to the water vapor density flux. Latent and sensible heat fluxes were measured every 30 minutes. The height of the eddy covariance system was 1.8 m from the ground and the orientation of the system was 212° toward southwest. On DoY 109, the sensor was moved to a height of 2.71 m, with the same orientation. Table 3 shows the list of specifications of the CSAT3. Data collected by the eddy covariance system have been processed for coordinate rotation (Kaimal and Finnigan, 1994; Wilczak et al., 2001), WPL (Webb et al., 1980), oxygen (van Dijk et al., 2003), and sonic temperature corrections (Schotanus et al., 1983). Figure A-2 shows the processed latent and sensible heat fluxes observed during MicroWEX-5, and Figure A-6 shows wind speed and direction.

Figure 8. Eddy covariance system

Table 3. Specifications of the CSAT3 (Campbell Scientific, 1998)

Description	Value
Measurement rate	1 to 60 Hz
Noise equivalent wind	1 mm/sec in horizontal wind speed and 0.5 mm/sec in vertical wind speed
Wind measurement offset	< ±4 cm/sec over –30 to 50ºC
Output signals	Digital SDM or RS-232 and Analog
Digital output signal range	±65.535 m/sec in wind speed and 300 to 366 m/sec in speed of sound
Digital output signal resolution	0.25 to 2 mm/sec in vertical wind speed and 1 mm/s in speed of sound
Analog output signal range	±32.768 to ±65.536 m/sec in wind speed and 300 to 366 m/sec in speed of sound
Analog output signal resolution	±8.192 mm/sec in vertical wind speed and 16 mm/sec in speed of sound
Measurement path length	10.0 cm vertical and 5.8 cm horizontal
Transducer path angle from horizontal	60 degrees
Transducer	0.64 cm in diameter
Transducer mounting arms	0.84 cm in diameter
Support arms	1.59 cm in diameter
Dimensions: anemometer head	47.3 cm x 42.4 cm
Dimensions: electronics box	26 cm x 16 cm x 9 cm
Dimensions: carry case	71.1 cm x 58.4 cm x 33 cm
Weight: anemometer head	1.7 kg
Weight: electronics box	2.8 kg
Weight: shipping	16.8 kg
Operating temperature range	-30ºC to 50ºC
Power requirement: voltage supply	10 to 16 VDC
Power requirement: current	200 mA at 60 Hz measurement rate and 100 mA at 20 Hz measurement rate

4.3 Net Radiometer

A Kipp and Zonen CNR-1 four-component net radiometer (Figure 9) was located at the center of the field to measure up- and down-welling short- and long-wave infrared radiation. The sensor consists of two pyranometers (CM-3) and two pyrgeometers (CG-3). The sensor was installed at the height of 2.66 m above ground and facing south. Table 4 shows the list of specifications of the CNR-1 net radiometer. Figure A-3 shows the up- and down-welling short- and long-wave radiation observed during MicroWEX-5.

Figure 9. CNR-1 net radiometer

Table 4. Specifications of the CNR-1 net radiometer (Campbell Scientific, 2006a)

Description	Value
Measurement spectrum: CM-3	305 to 2800 nm
Measurement spectrum: CG-3	5000 to 50000 nm
Response time	18 sec
Sensitivity	10 to 35 μV/(W/m^2)
Pt-100 sensor temperature measurement	DIN class A
Accuracy of the Pt-100 measurement	± 2 K
Heating	Resistor 24 ohms, 6 VA at 12 volt
Maximum error due to heating: CM-3	10 W/m^2
Operating temperature	-40º to 70ºC
Daily total radiation accuracy	± 10%
Cable length	10 m
Weight	4 kg

4.4 Precipitation

Precipitation was determined using four tipping-bucket raingages, two on either side of the radiometer footprints and two on either side of the field. The West footprint raingage failed soon after the experiment started. Figure A-4 shows the observed precipitation.

4.5 Air Temperature and Relative Humidity

Air temperature and relative humidity were measured every 15 minutes at the Northwest station using a Campbell Scientific HMP45C Temperature and Relative Humidity Probe. Figure A-5 shows the relative humidity and air temperature observations during MicroWEX-5 at a height of 2.0 m. Table 5 shows the list of specifications.

Table 5. Specifications of the HMP45C (Campbell Scientific, 2006c)

Description	Value
Temperature Range	-40º to 60ºC
Temperature Accuracy	0.2º (-40ºC) to 0.5º (20ºC)
Relative Humidity Range	0 to 100%
Relative Humidity Accuracy @ 20ºC	2% (0-90%) to 3% (90-10%) RH
RH Response to Temperature	0.05% RH/ºC
Response Time	15 seconds at 20ºC, 90%RH
Temperature Measurement	1000 Ω PRT, IEC 751 1/3 Class B
Relative Humidity Measurement	HUMICAP 180

4.6 Canopy Air Temperature

Air temperature, at six heights within the canopy, was measured every 15 minutes at the Northwest station using thermistors on a PVC pipe, as shown in Figure 10. The heights were adjusted as the canopy grew, listed in Table 6. Figures A-7 through A-9 show the observations of canopy temperature during MicroWEX-5.

Table 6. Canopy thermistor heights

DoY	Measurement heights (cm)
72	0,5,10,15,20,25
102	0,5,10,15,30,40
109	0,15,30,45,60,75
114	0,40,60,80,100,120
118	0,40,85,110,135,160
125	0,40,75,110,145,180

Figure 10. Canopy thermistors.

4.7 Soil Moisture and Temperature Probes

Twenty-eight Campbell Scientific time-domain water content reflectometers (CS616) were used to measure soil volumetric water content of 2, 4, 8, 16, 32, 64, and 120 cm every 15 minutes. At the East station, there were also two deep TDRs, one each by the Northeast and Southeast wells at approximately 1.6 m. At the Northwest station, the deep sensor was by the Northwest well at 1.45 m, the Southwest deep TDR was at 1.8 m. The observations of soil moisture were duplicated at the depth of 2 cm. One of the Northwest thermistors gave spurious results and the East station 2 cm thermistor failed less than 24 hours after it was installed, so the data from these sensors were not included. The calibration coefficients for the CS616 probes are listed in Table 7. Figure A-10 shows the soil temperatures observed at the depths of 2 cm, 4 cm, 8 cm, 16 cm, 32 cm, 64 cm, and 120 cm, at Northwest station during MicroWEX-5. Figure A-11 and A-12 show the soil temperatures observed at the same depths at the Southwest station and East station. Figure A-13, A-14, and A-15 show the volumetric soil moisture content observed at the same depths plus the deep TDRs for the Northwest, Southwest, and East stations respectively.

Table 7. The calibration coefficients for the CS616 probes (Campbell Scientific, 2006b)

Coefficient	Value
C_0	-0.187
C_1	0.037
C_2	0.335

4.8 Soil Heat Flux Plates

Two Campbell Scientific soil heat flux plates (HFT-3) were used to measure soil heat flux at the depth of 2 cm at the Northwest station. The Eddy Covariance System, East, and Southwest stations each had one SHF plate at 2cm, though the observations from the soil heat flux plate near the Eddy Covariance System were significantly higher than the ones at the Northwest, East, and Southwest stations. The data from the Eddy Covariance System soil heat flux plates are not included. Figure A-16 shows the soil heat fluxes observed at all locations.

5. SOIL SAMPLING

5.1 Soil Surface Roughness

Soil roughness was measured near the radiometer footprints at the beginning (DoY 69) and end (DoY 150) of the season by Dr. Clint Slatton and Mr. Juan Fernandez from the Geosensing Systems Engineering group at the Civil Engineering Dept. at UF, using a 3D laser scanner for both days (Figure 11a) and also with a traditional grid board method for DoY 69 (Figure 11b). Jang et al., 2006, describes the grid board method in detail. The 3D scanning laser technology was the ILRIS-36D, developed in Canada by Optech. Specifications are given in Table 8. Figure A-17 shows roughness profiles from both methods from DoY 69 and Figure A-18 shows the ILRIS scan on DoY 150.

Table 8. Specifications of the Optech ILRIS-36D.

Description	Value
Range	3 – 1500 m (reflectivity 4 – 80%)
Wavelength	1535 nm
Pulse width	<10 ns
Pulse energy	<10 μm
Minimum sample separation	0.00115º
Scanning speed	2,000 points/s
Accuracy	4 mm
Point spacing	1 cm

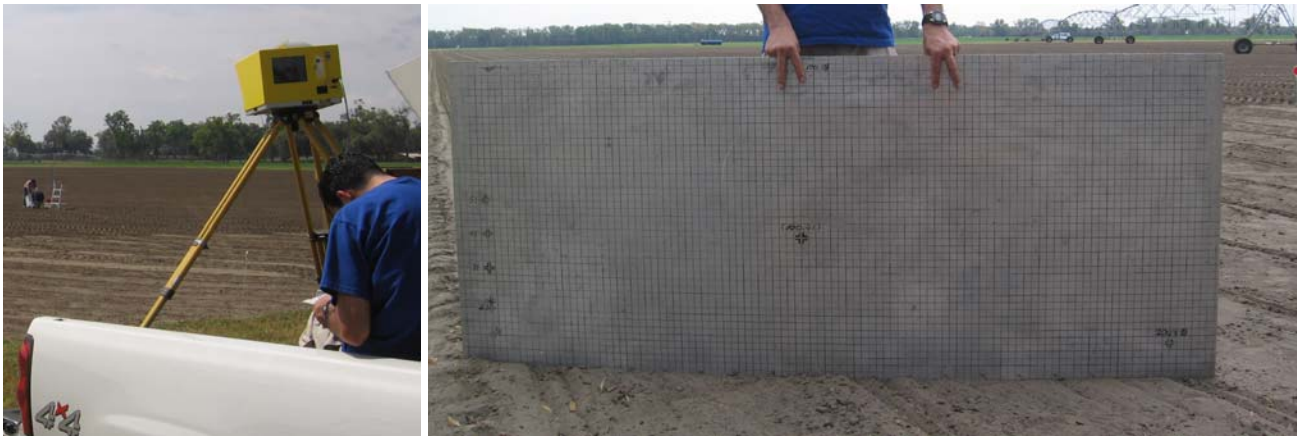

Figure 11. a) Laser scanner and b) grid board for soil roughness measurements.

6. VEGETATION SAMPLING

Vegetation properties such as stand density, row spacing, height, biomass, and LAI were measured weekly during the field experiment. The crop density derived from the stand density and row spacing was measured at the first two sampling since the corn seeds were planted in the fixed spacing and the germination rate is over 70% throughout the field. The specific weekly measurements include height, biomass, and LAI. In the whole season, the vegetation samplings were conducted on four spatially distributed sampling locations (Figure 3). It was designed to characterize the spatial variability of the vegetation properties in the study site.

6.1 Height and Width

Crop height and width were measured by placing a measuring stick at the soil surface to average height of the crop. Four representative plants were selected to obtain heights inside each vegetation sampling area. Crop height for each of the sampling areas is shown in Figure A-19.

6.2 LAI

LAI was measured with a Li-Cor LAI-2000 in the inter-row region with 4 cross-row measurements. The LAI-2000 was set to average 2 locations into a single value for each vegetation sampling area so one observation was taken above the canopy and 4 beneath the canopy; in the row, ¼ of the way across the row, ½ of the way across the row, and ¾ of the way across the row. This gave a spatial average for row crops of partial cover. LAI for each of the sampling areas is shown in Figure A-20.

6.3 Green and Dry Biomass

Each biomass sampling included one row. The sampling length was measured the same as length during stand density measurement. The sample started in-between two plants and ended at the next midpoint that is also greater than or equal to one meter away from the starting point. The plants within this length were cut at the base, separated into leaves, stems, and ears, and weighed immediately. The samples were dried in the oven at 70ºC for 48 hours and their dry weights were measured, separating the ears into husks, shucks, and kernel/cobs. Figure A-21 shows the Green and Dry biomass observed during MicroWEX-5. Dry biomass at harvest is used as yield.

6.4 Vertical Distribution of Moisture in the Canopy

Details of the methods and measurements can be found in Casanova et al. 2006.

7. WELL SAMPLING

7.1 Groundwater sampling

The groundwater sampling was conducted by Dr. Michael Dukes and his research team. The sampling was conducted at all four wells in the field at the end of each month from March to June in 2006. The groundwater sampling included groundwater level measurement by water level sounder, and collecting groundwater samples for the analysis of N_2. Figure A-22 shows the observations of N_2 during MicroWEX-5.

7.2 Water level measurement

The water level measurement was processed by the Levelogger from Solinst Canada Ltd.. The Leveloggers were installed at each well and set to automatically record the water level every 15 minutes. The data were downloaded onto a laptop during the well sampling at the end of each month. Figure A-23 shows the water table elevation and depth during MicroWEX-5. The data from the Southeast Levelogger were severely corrupted due to a problem in the communication hardware, and could not be included.

8. FIELD LOG

Note: Time is in Eastern Standard Time.

March 9 (DoY 68)

08:15	Planting began; finished by the end of the day
08:40	Planting in L-band footprint done
09:41	Planting in C-band footprint done
	C-band cal/antenna voltages tracking each other; antenna/cal switch replaced

March 10 (DoY 69)

	Northwest station sensors installed (CNR, TIR, HMP45C, soil thermistors, TDRs)
	CNR was temporarily without anti-dew heating, also not level
	Soil roughness measurement with LIDAR and grid-board

March 11 (DoY 70)

13:00	C-band radiometer calibration
14:00	L-band radiometer calibration

March 13 (DoY 72)

	Setup eddy covariance, East, and Southwest stations
	Replaced 2 Northwest thermistors: 2 cm near L-band footprint and 8 cm
	Installed canopy thermistors (0, 5, 10, 15, 20, 25 cm)
	Northwest data collection begins

March 14 (DoY 73)

	Leveled CNR
	Installed East and Southwest stations; data collection begins
	Installed eddy covariance soil heat flux plate
09:30	L-band angle incorrect due to press-fit slippage on angle-iron rotator; stopped data collection and brought it down

March 15 (DoY 74)

10:00	L-band rotator welded into correct position; brought up the radiometer and restarted
	Marked areas for vegetation sampling
	Less than 50% emergence

March 16 (DoY 75)

13:00	C-band radiometer calibration
14:00	L-band radiometer calibration

March 17 (DoY 76)

08:00	Herbicide sprayed; radiometers brought down
09:00	Radiometers brought up

March 18 (DoY 77)

	Found East station fallen to the ground; data unaffected
	Installed soil water potential sensors in Northwest at depth of 32cm
	Hand planted areas around sensors and wells

March 19 (DoY 78)

09:00	C-band radiometer calibration
10:00	L-band radiometer calibration

March 20 (DoY 79)

10:00	Repaired East station tripod

March 21 (DoY 80)

09:30	Brought down L-band and removed mylar cover to avoid dew
10:00	L-band back up

March 22 (DoY 81)

09:00	Vegetation sampling (#1)
10:45	L-band set too low by one rung (~15") after mylar removal, moved up one rung; data unaffected.
	Soil water potential sensors connected to Northwest datalogger

March 24 (DoY 83)

1:00	C-band radiometer calibration and changed desiccants
2:00	L-band radiometer calibration and changed desiccants

March 31 (DoY 90)

11:00	C-band radiometer calibration
12:00	L-band radiometer calibration

April 5 (DoY 95)

10:30	Vegetation sampling (#2)
	East station found to be tilted; data unaffected

April 7 (DoY 97)

10:00	C-band radiometer calibration
11:00	L-band radiometer calibration
12:00	Canopy thermistors' height changed (0, 5, 10, 15, 30, 40 cm)

April 10 (DoY 100)

09:00	Vertical distribution of moisture sampling (#1)

April 12 (DoY 102)

14:30	Vegetation sampling (#3)
16:00	Canopy thermistors' height changed (0, 5, 20, 35, 45, 55 cm)

April 14 (DoY 104)

12:00	Changed desiccants
12:30	C-band radiometer calibration
13:00	L-band radiometer calibration

April 17 (DoY 107)

10:30	Repaired Styrofoam shield on L-band; data unaffected

April 19 (DoY 109)

10:00	CSAT height changed from 1.8m to 2.71m
11:30	Canopy thermistors' height changed (0, 15, 30, 45, 60, 75 cm)
	Gap in Southwest station memory began, from DoY 109 - 121
12:30	Vegetation sampling (#4)

April 21 (DoY 111)

09:30	C-band radiometer calibration
10:30	L-band radiometer calibration

April 24 (DoY 114)

09:30	Clean KH2O windows; DoY 109.5 to DoY 114.42 data bad
09:45	Canopy thermistors' height changed (0, 40, 60, 80, 100, 120 cm)

April 25 (DoY 115)

	2 cm thermistor added to East station
	8 cm thermistor added to Southwest station

April 26 (DoY 116)

09:30	Vegetation sampling (#5)
	2 cm thermistor added to East station buried; data collection

	started; failed later today. All data collected should be ignored.
	8 cm thermistor added to Southwest station buried; data collection started
	Tassel formation beginning

April 28 (DoY 118)

10:30	Changed desiccants
11:00	C-band radiometer calibration
11:30	L-band radiometer calibration
11:30	Canopy thermistors' height changed (0, 40, 85, 110, 135, 160 cm)

May 1 (DoY 121)

09:00	Vertical distribution of moisture sampling (#2)
	Tassel formation for greater than 75% of the field
	Ear formation for roughly 75% of the field

May 3 (DoY 123)

09:30	Vegetation sampling (#6)
	Tassel formation for 100% of the field
	Silking for some of the field

May 5 (DoY 125)

	Silking for between 50 and 75% of the field
11:00	C-band radiometer calibration
11:30	L-band radiometer calibration
11:30	Canopy thermistors' height changed (0, 40, 75, 110, 145, 180 cm)

May 10 (DoY 130)

10:00	Vegetation sampling (#7)
	Silking for greater than 75% of the field

May 12 (DoY 132)

	Vegetation samples (#7) found burned in oven
10:30	Changed desiccants
11:00	C-band radiometer calibration
11:30	L-band radiometer calibration

May 15 (DoY 135)

10:30	Cleaned KH2O windows
12:00	Vertical distribution of moisture sampling (#3)

May 18 (DoY 138)

12:00	Vegetation sampling (NW and NE only) (#8)

May 19 (DoY 139)

09:00	C-band radiometer calibration
09:30	L-band radiometer calibration

May 20 (DoY 140)

12:30	Ears removed from L- and C- band radiometer footprints

May 24 (DoY 144)

09:00	Leaves removed from L- and C- band radiometer footprints

May 25 (DoY 145)

10:00	Vegetation sampling (#9)

May 26 (DoY 146)

09:00	C-band radiometer calibration
09:30	L-band radiometer calibration
	East, Southwest, and eddy covariance stations removed

May 30 (DoY 150)

	Soil roughness measurement of footprints with LIDAR
	Final sensor removal

June 5 (DoY 156)

12:00	Changed desiccants
12:00	C-band radiometer calibration
12:30	L-band radiometer calibration

9. REFERENCES

Campbell Scientific, *CSAT3 Three Dimensional Sonic Anemometer Instruction Manual*, Campbell Scientific Inc., Logan, UT, 1998.

Campbell Scientific, *HFT3 soil heat flux plate instruction manual*, Campbell Scientific Inc., Logan, UT, 2003.

Campbell Scientific, *CNR1 Net Radiometer Instruction Manual*, Campbell Scientific Inc., Logan, UT, 2006a.

Campbell Scientific, *CS615 andCS625 water content reflectometers instruction manual*, Campbell Scientific Inc., Logan, UT, 2006b.

Campbell Scientific, *Campbell Scientific Model HMP45C Temperature and Relative Humidity Probe instruction manual,* Campbell Scientific Inc., Logan, UT, 2006c.

Casanova, J., J. Judge, and M. Jang, 2006. Vertical Distribution of Moisture in a Growing Sweet Corn Canopy During Center for Remote Sensing, University of Florida, Available at UF/IFAS Web site at http://edis.ifas.ufl.edu/AE395, Circular No 1483.

Jang, M., K.J.C. Tien, J. Casanova, and J. Judge, 2006. Measurements of Soil Roughness During the Fourth Microwave Water and Energy Balance Experiment: April 18 through June 13, 2005, Center for Remote Sensing, University of Florida, Available at UF/IFAS Web site at http://edis.ifas.ufl.edu/AE363, Circular No 1483.

J. C. Kaimal and J. J. Finnigan, *Atmospheric Boundary Layer Flows*, Oxford University Press, New York, NY, 1994.

R. D. De Roo, Personal communication, February, 2007.

R. D. De Roo, *University of Florida C-band Radiometer Summary*, Space Physics Research Laboratory, University of Michigan, Ann Arbor, MI, March, 2002.

R. D. De Roo, *TMRS-3 Radiometer Tuning Procedures*, Space Physics Research Laboratory, University of Michigan, Ann Arbor, MI, March, 2003.

P. Schotanus, F. T. M. Nieuwstadt, and H. A. R. DeBruin, "Temperature measurement with a sonic anemometer and its application to heat and moisture fluctuations," *Bound.-Layer Meteorol.*, vol. 26, pp. 81-93, 1983.

A. van Dijk, W. Kohsiek, and H. A. R. DeBruin, "Oxygen sensitivity of krypton and Lyman-alpha hygrometer," *J. Atmos. Ocean. Tech.*, vol. 20, pp. 143-151., 2003.

E. K. Webb, G. I. Pearman, and R. Leuning, " Correction of flux measurements for density effects due to heat and water vapor transfer," *Quart. J. Roy. Meteorol., Soc.*, vol. 106, pp. 85-100, 1980.

J. M. Wilczak, S. P. Oncley, and S. A. Stage, "Sonic anemometer tilt correction algorithms," *Bound.-Layer Meteorol.*, vol. 99, pp. 127-150, 2001.

10. ACKNOWLEDGEMENTS

This research was supported by funding obtained from the NASA-NIP Grant #00050655 and NSF Earth Science Directorate (EAR-0337277). The authors would like to thank Mr. Jim Boyer and his team at the PSREU for land and crop management.

A. FIELD OBSERVATIONS

Figure Captions

Figure A-1 Microwave brightness at vertical and horizontal polarizations……. ……..23
Figure A-2 Latent and sensible heat fluxes…….24
Figure A-3 Down- and up- welling short- and long- wave radiation…….…….25
Figure A-4 Precipitation ….……....26
Figure A-5 RH, Air temperature……..……....27
Figure A-6 Wind speed and direction……..……....28
Figure A-7 Canopy air temperature, 0.0 – 0.3 m…….29
Figure A-8 Canopy air temperature, 0.35 – 0.8 m..…….30
Figure A-9 Canopy air temperature, 0.85 – 1.8 m..…….31
Figure A-10 Northwest station soil temperature…….…….…….32
Figure A-11 Southwest station soil temperature.…...……..…….…...33
Figure A-12 East station soil temperature……..……....34
Figure A-13 Northwest station soil moisture……...35
Figure A-14 Southwest station soil moisture……...…….……...36
Figure A-15 East station soil moisture……..……..…….37
Figure A-16 Northwest, East, and Southwest station soil heat fluxes……..……...……38
Figure A-17 Soil Roughness Profiles, DoY 69……..…….39
Figure A-18 Soil Roughness Profiles, DoY 150…….40
Figure A-19 Canopy height……..……..…….41
Figure A-20 Canopy LAI……..……..…….42
Figure A-21 Wet and dry canopy biomass……..43
Figure A-22 Nitrogen sampling..……...……..…….44
Figure A-23 Water table depth and elevation above sea level……45

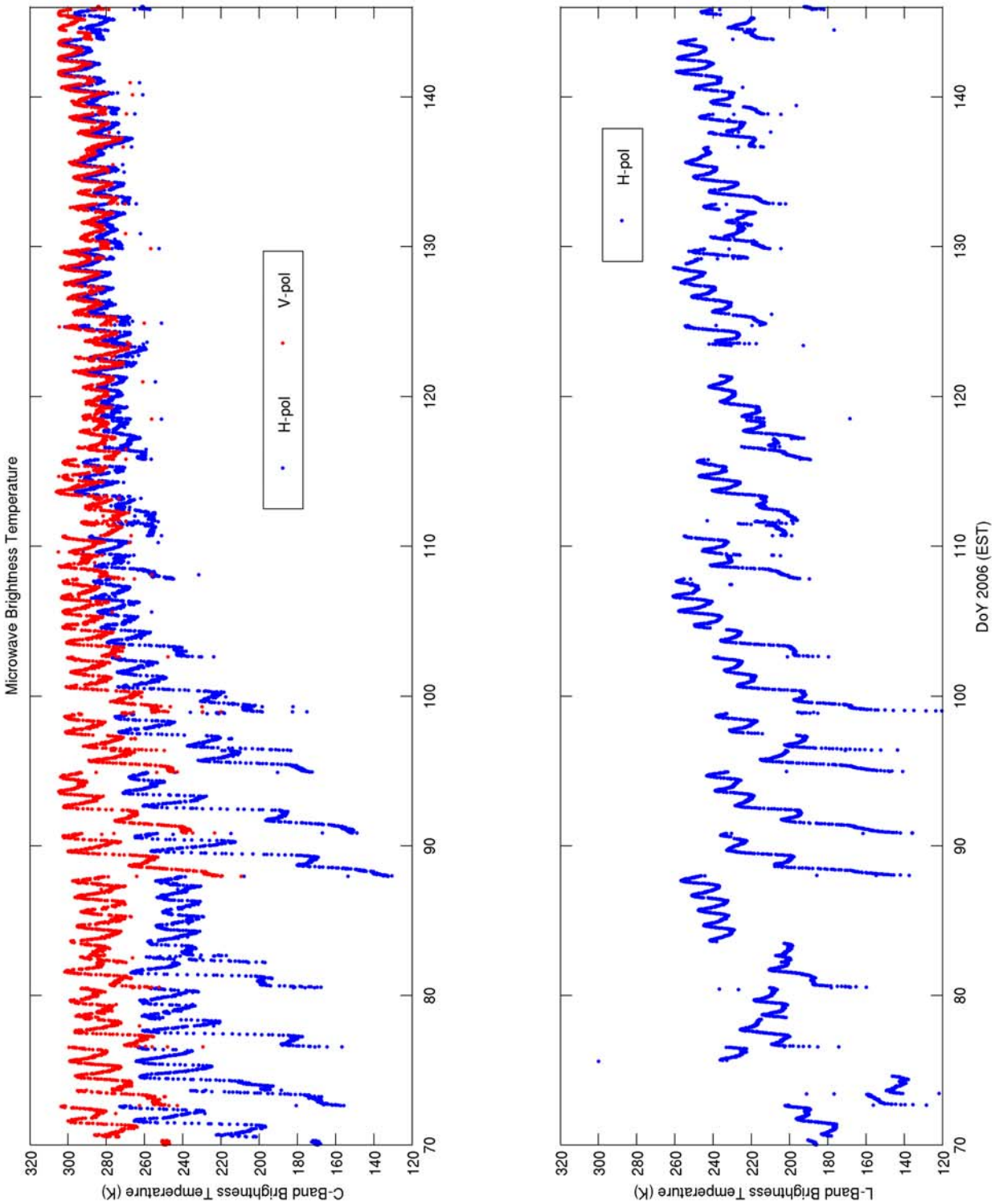

Figure A- 1 Microwave brightness at vertical and horizontal polarizations

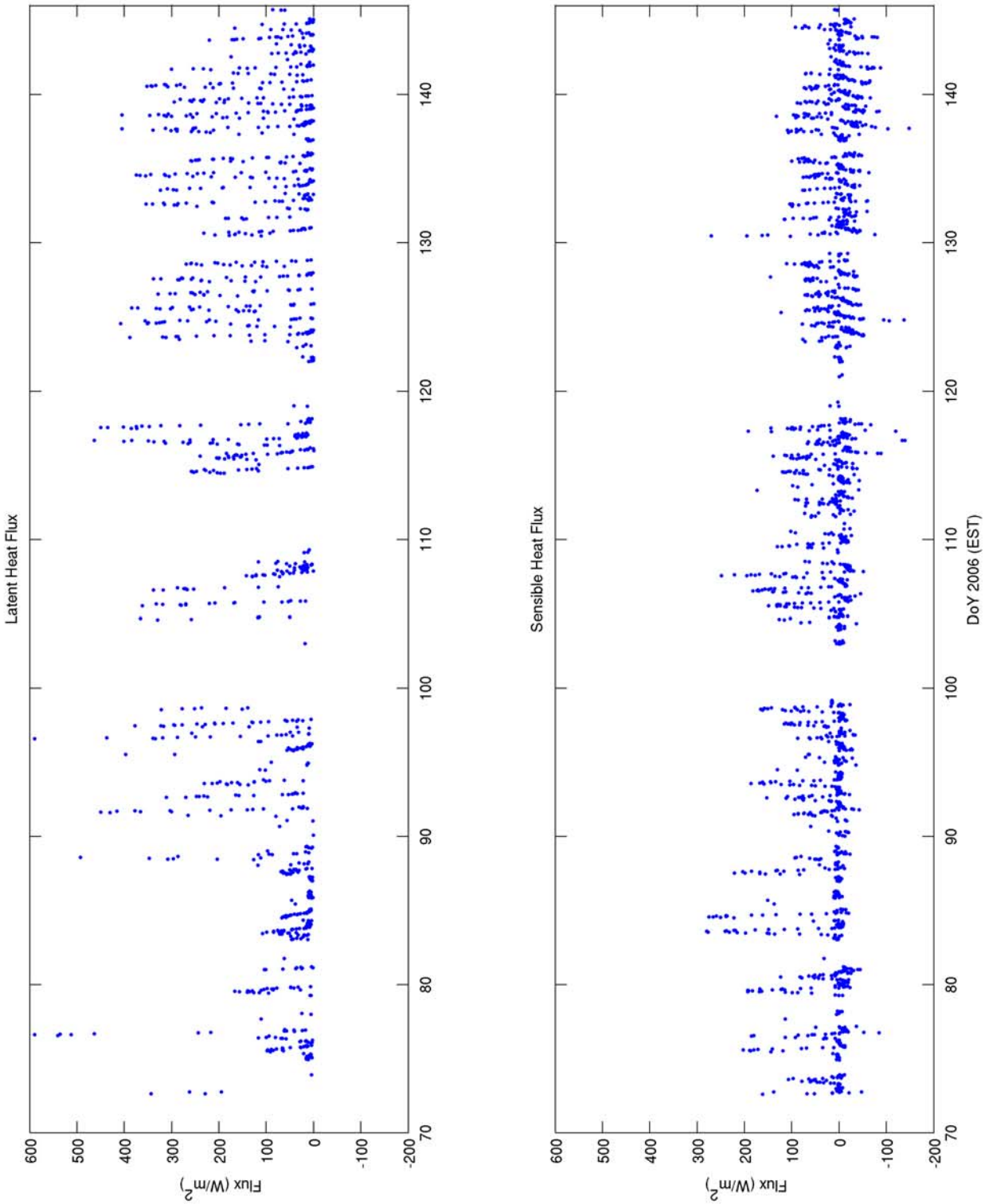

Figure A- 2 Latent and sensible heat fluxes

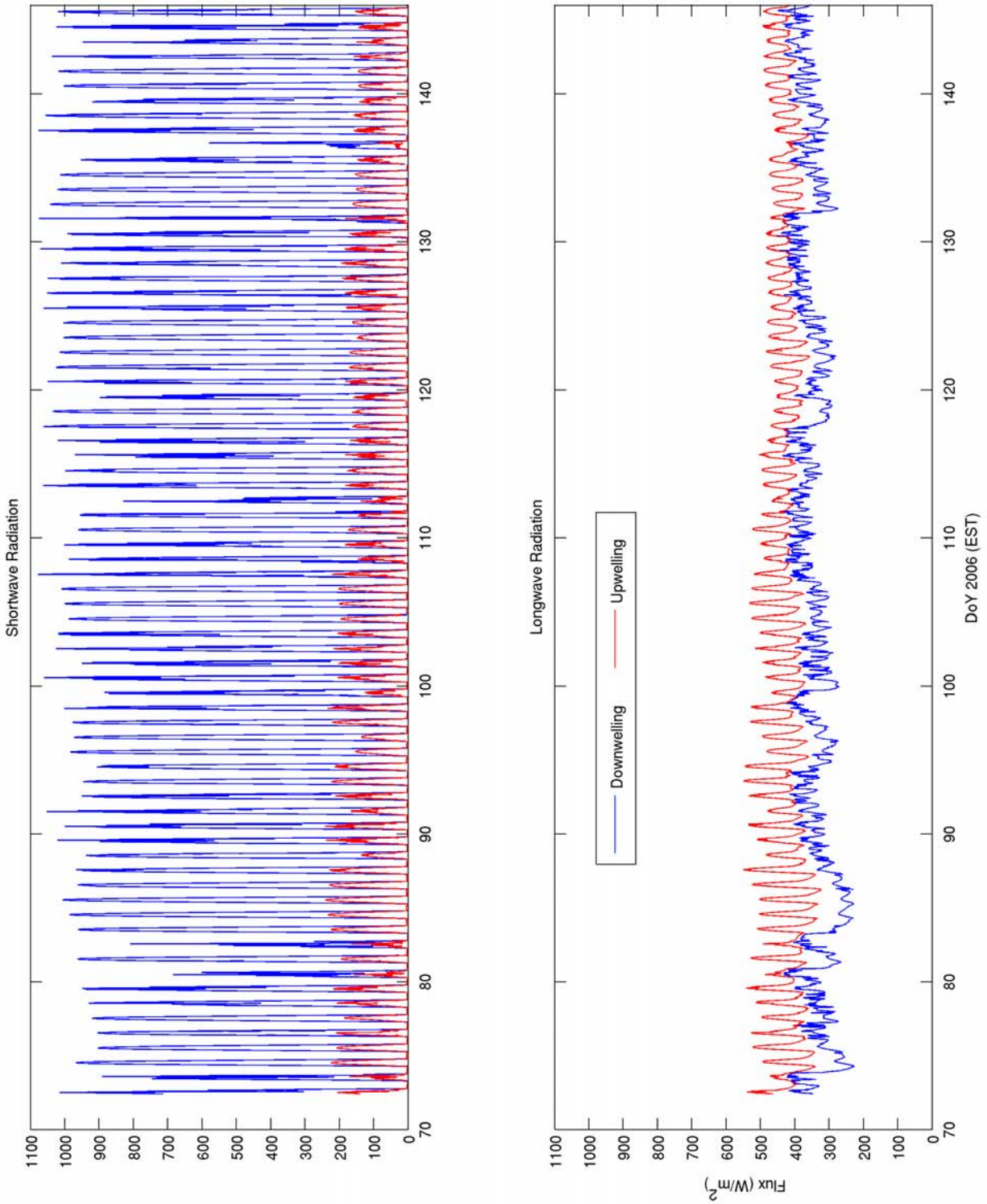

Figure A- 3 Down- and up- welling short- and long- wave radiation

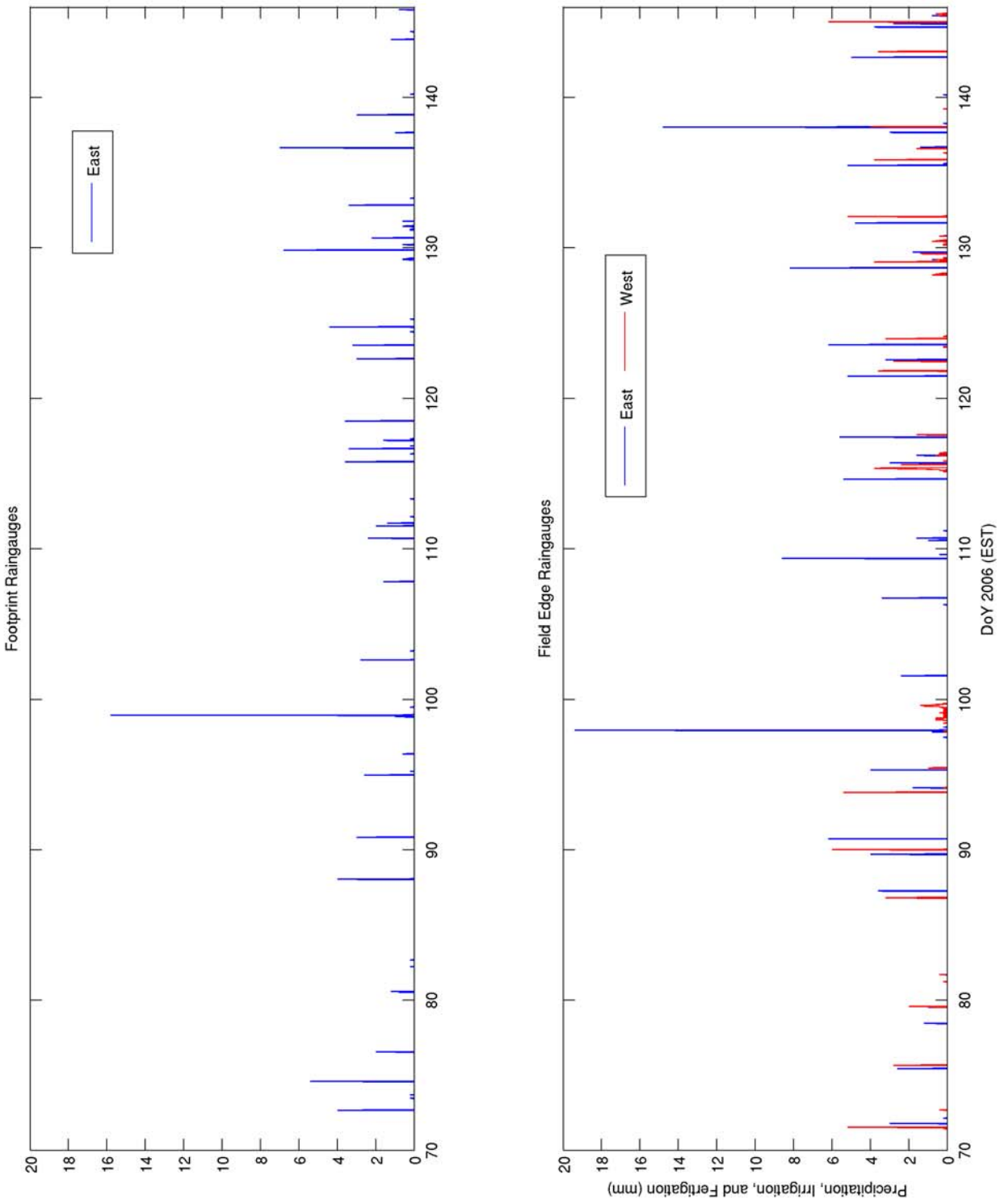

Figure A- 4 Precipitation

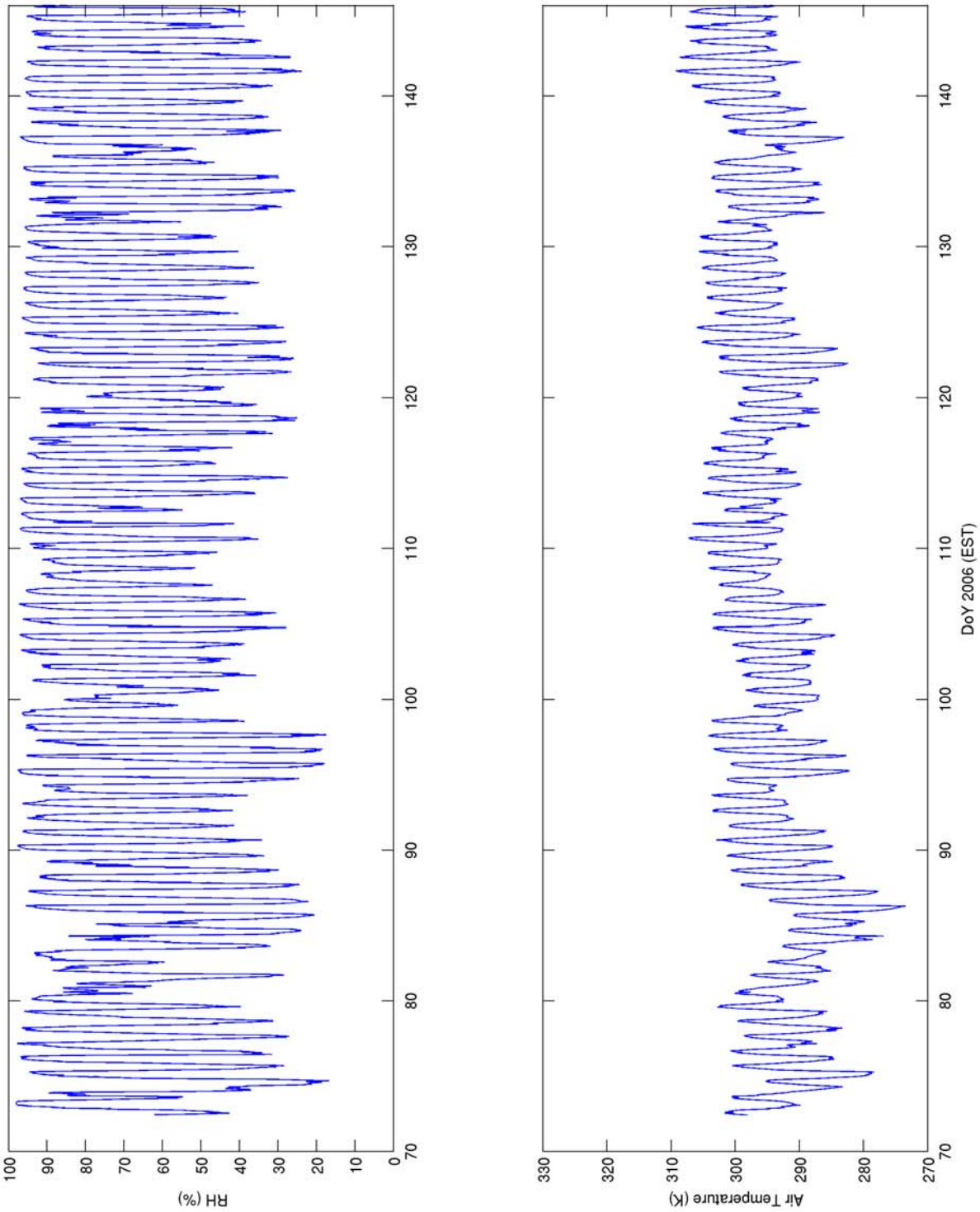

Figure A- 5 RH, air temperature.

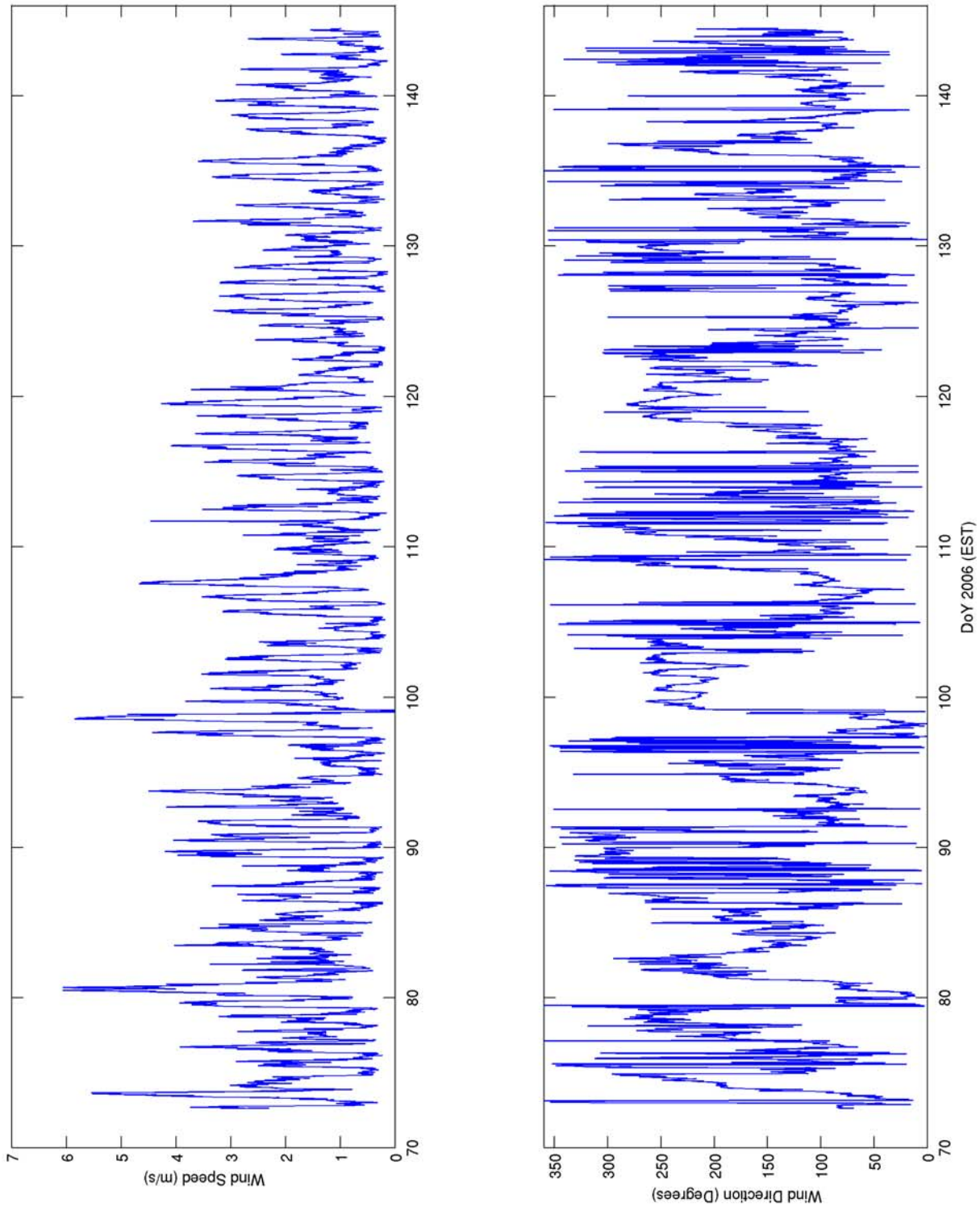

Figure A- 6 Wind speed and direction

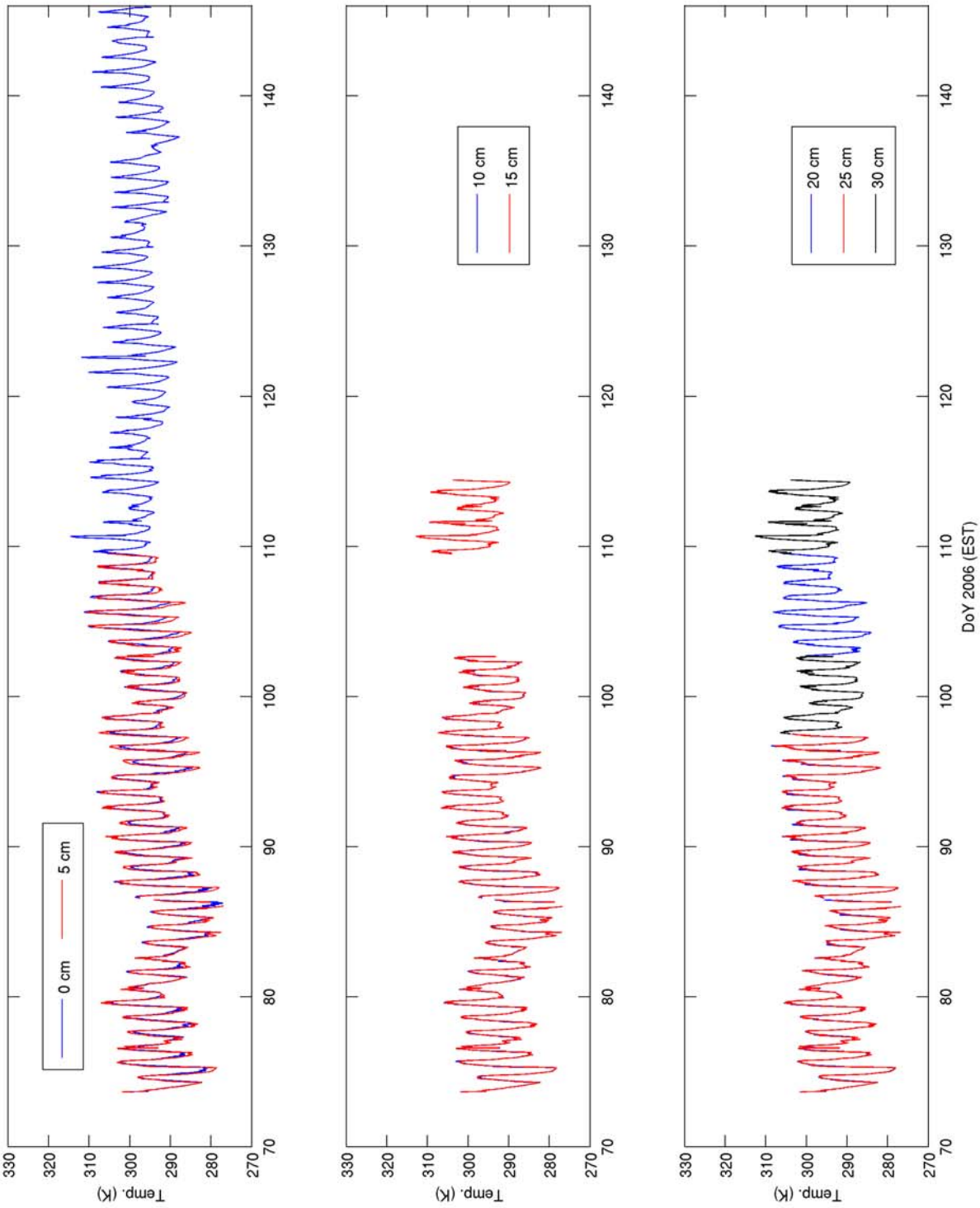

Figure A- 7 Canopy air temperature, 0.0 – 0.3 m

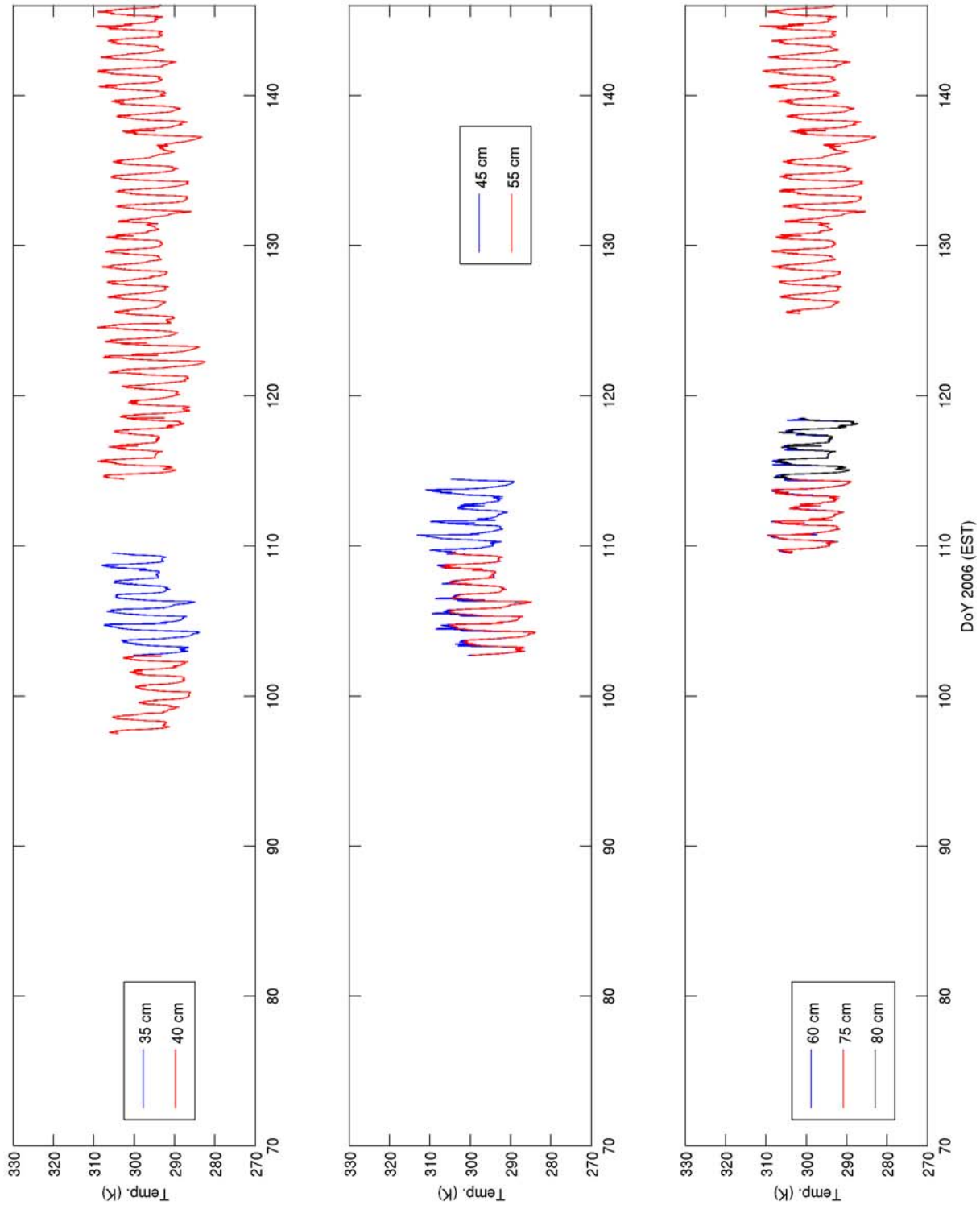

Figure A- 8 Canopy air temperature, 0.35 – 0.8 m

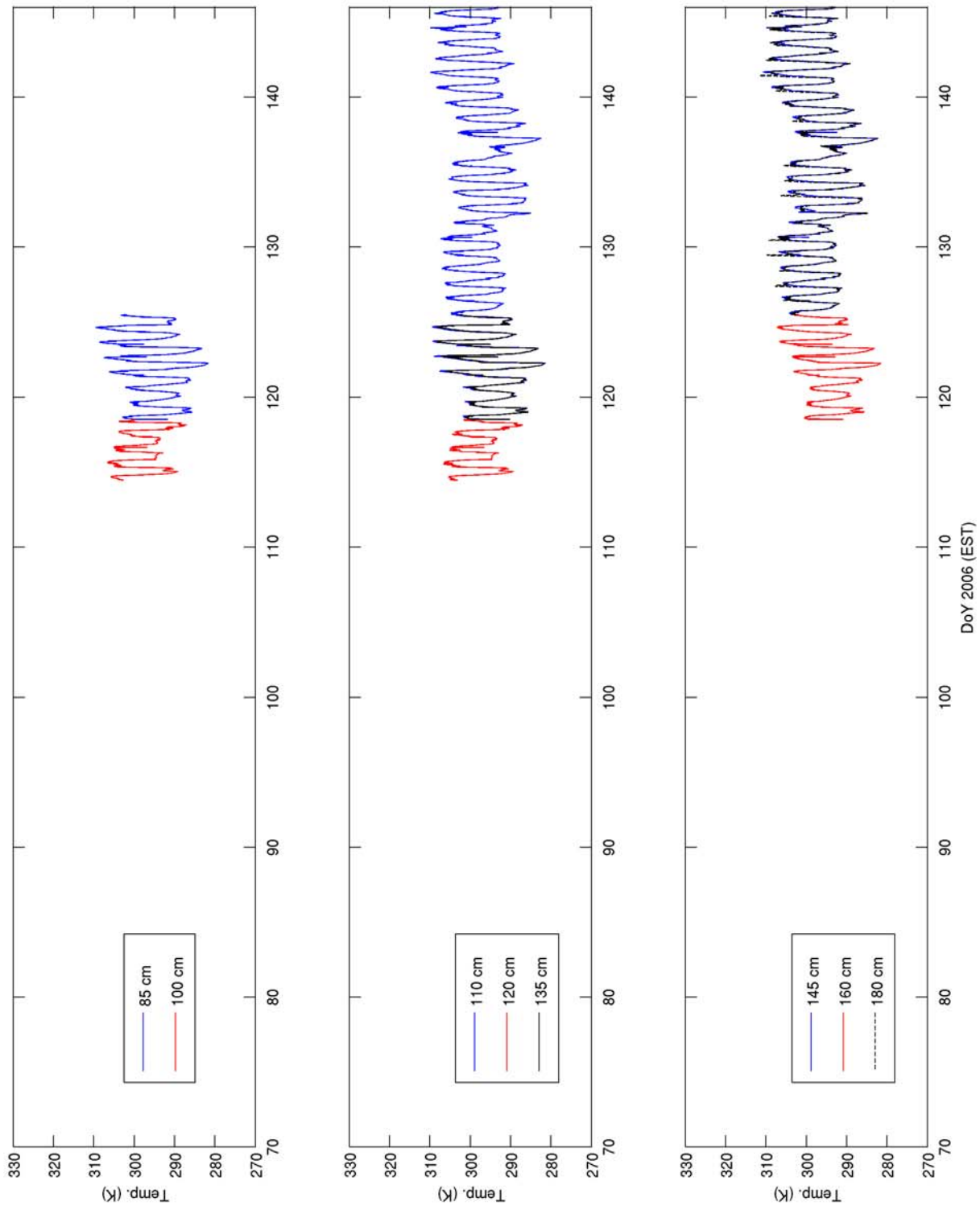

Figure A- 9 Canopy air temperature, 0.85 – 1.8 m

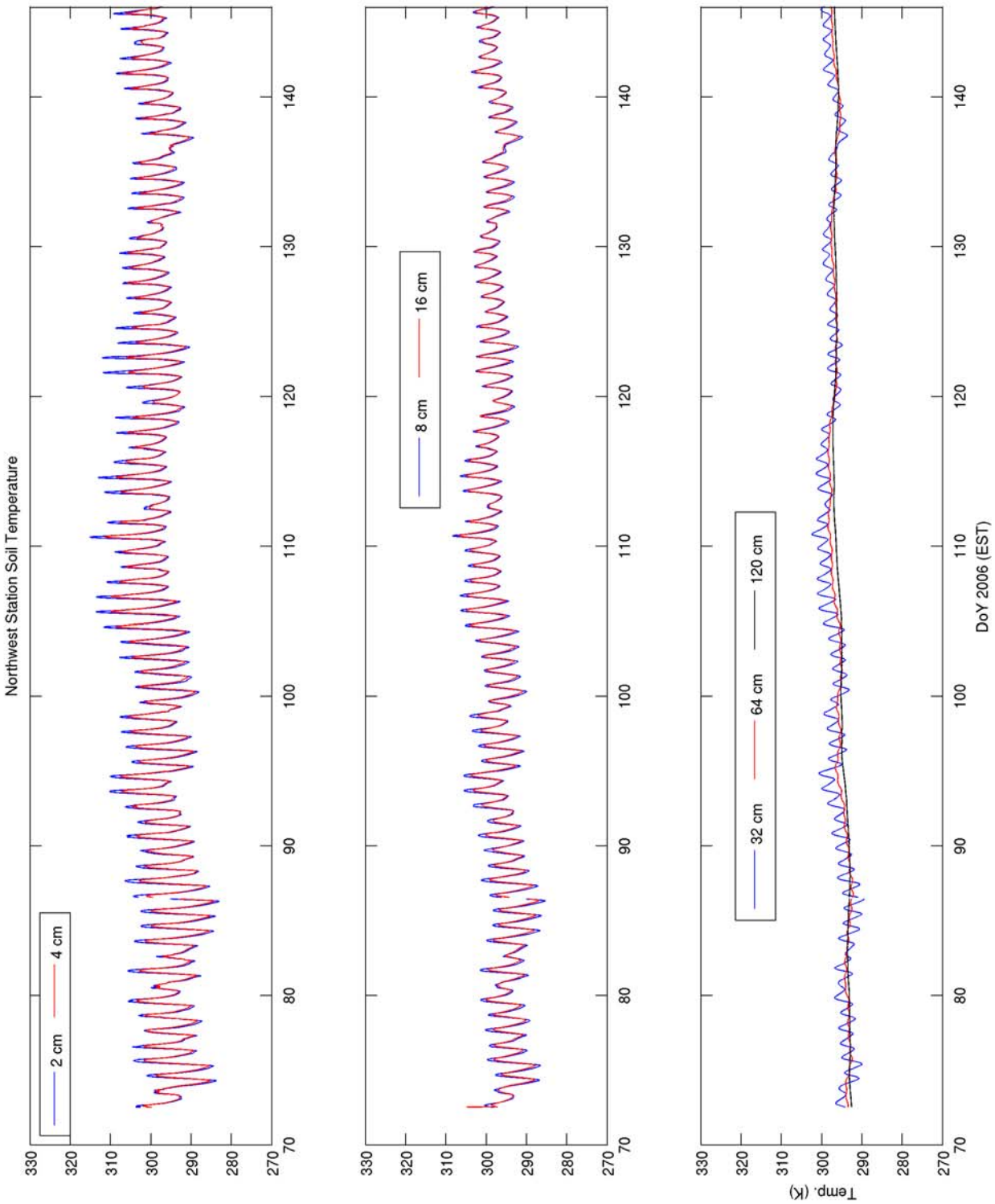

Figure A- 10 Northwest station soil temperature

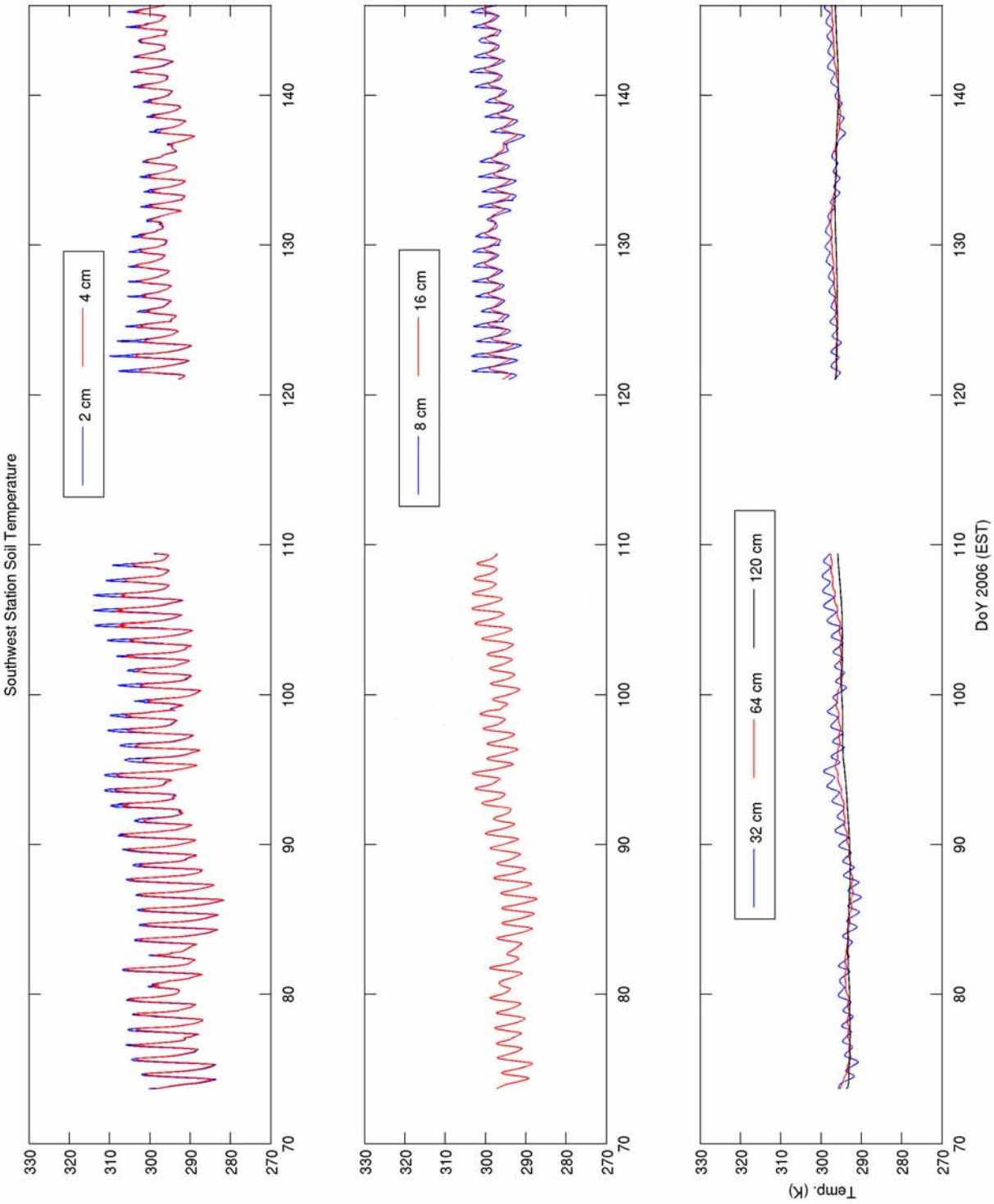

Figure A- 11 Southwest station soil temperature

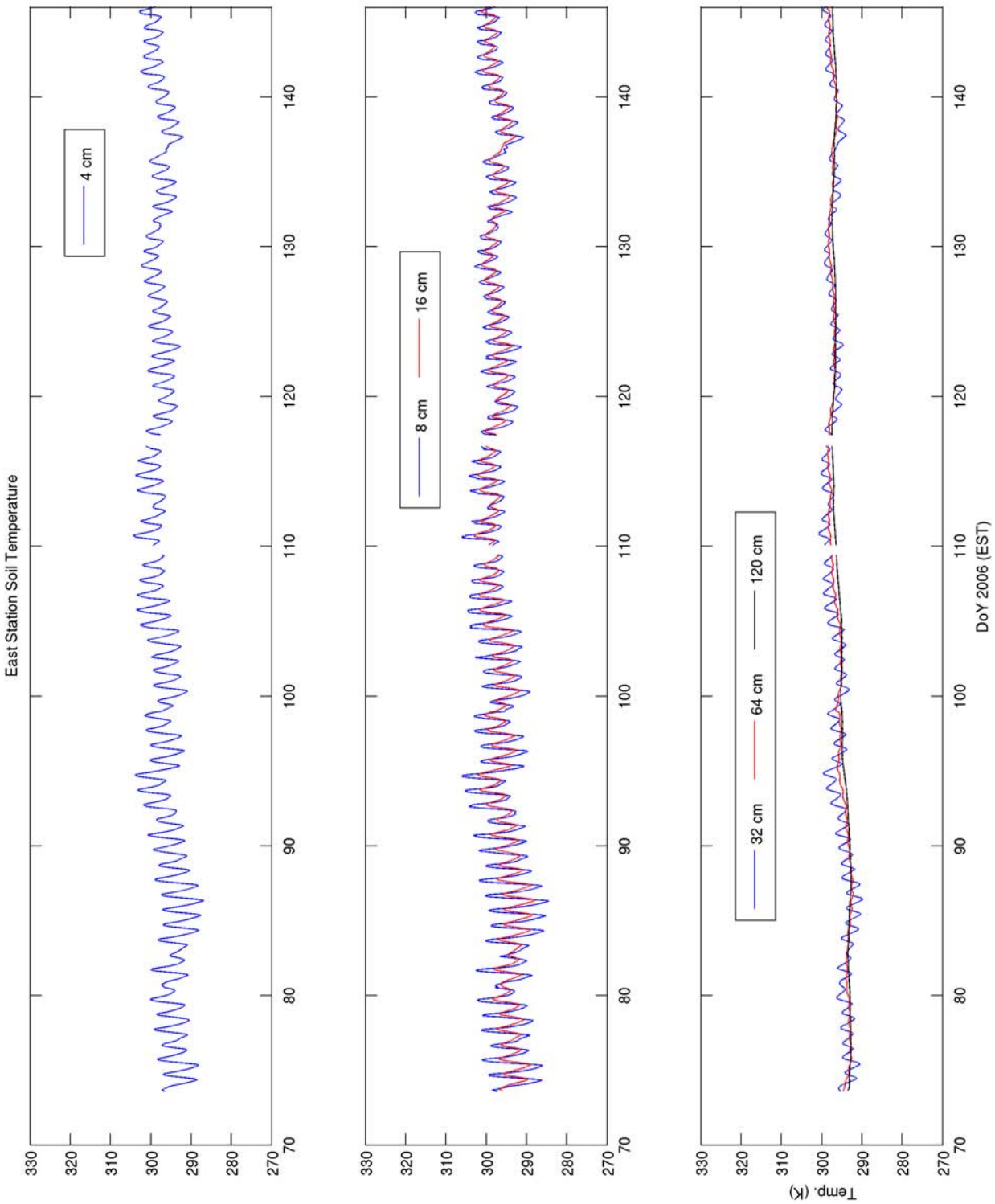

Figure A- 12 East station soil temperature

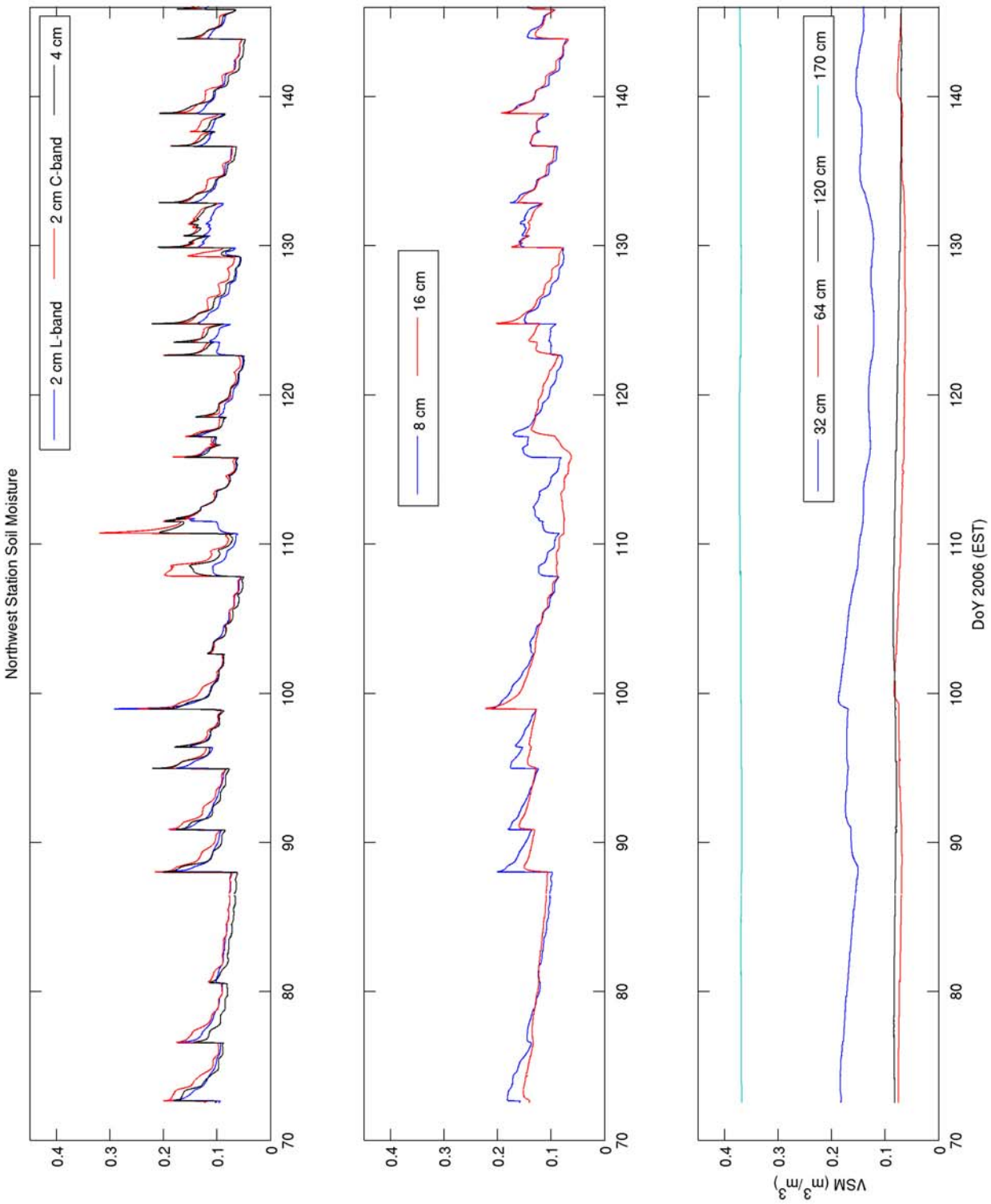

Figure A- 13 Northwest station soil moisture

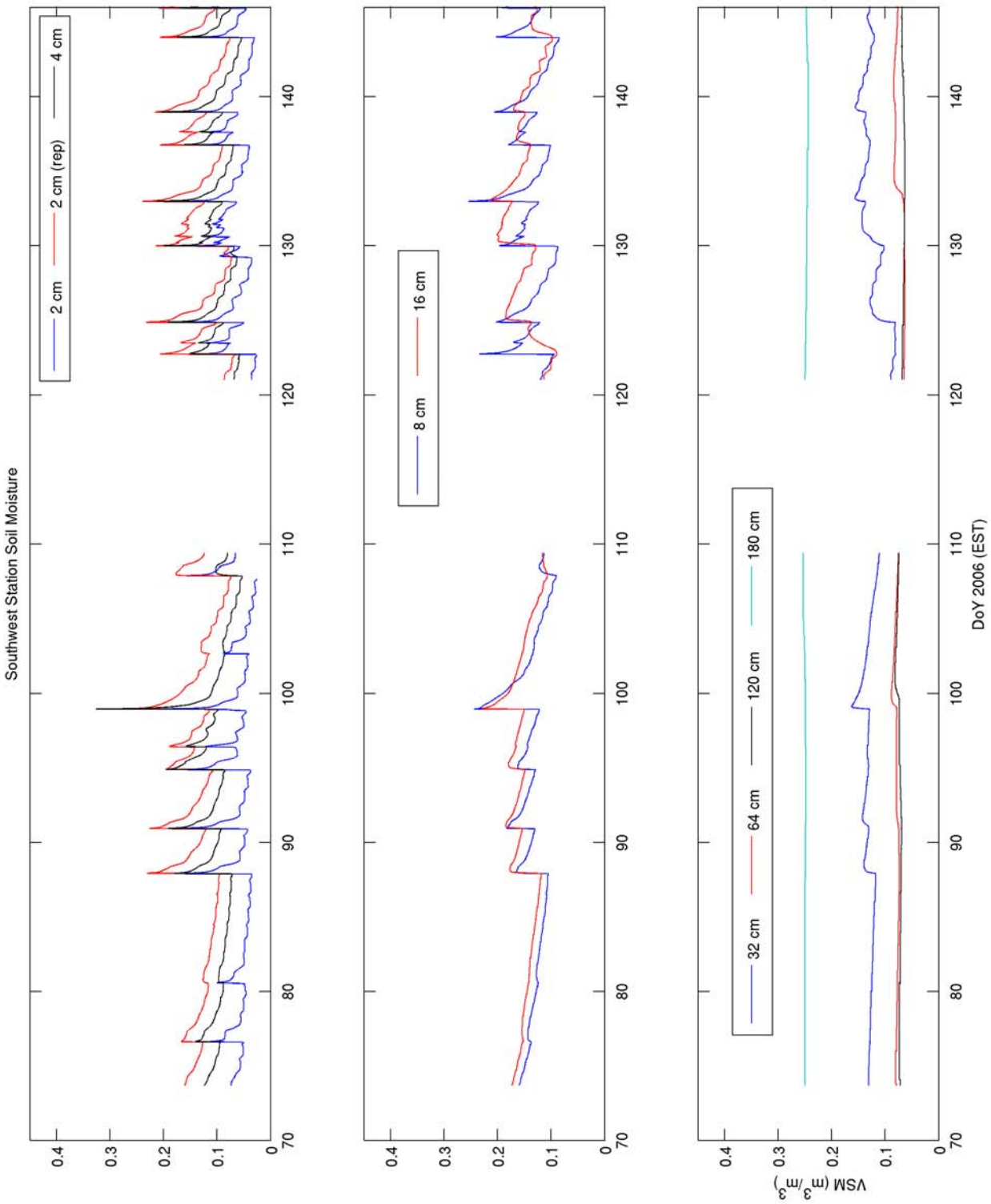

Figure A- 14 Southwest station soil moisture

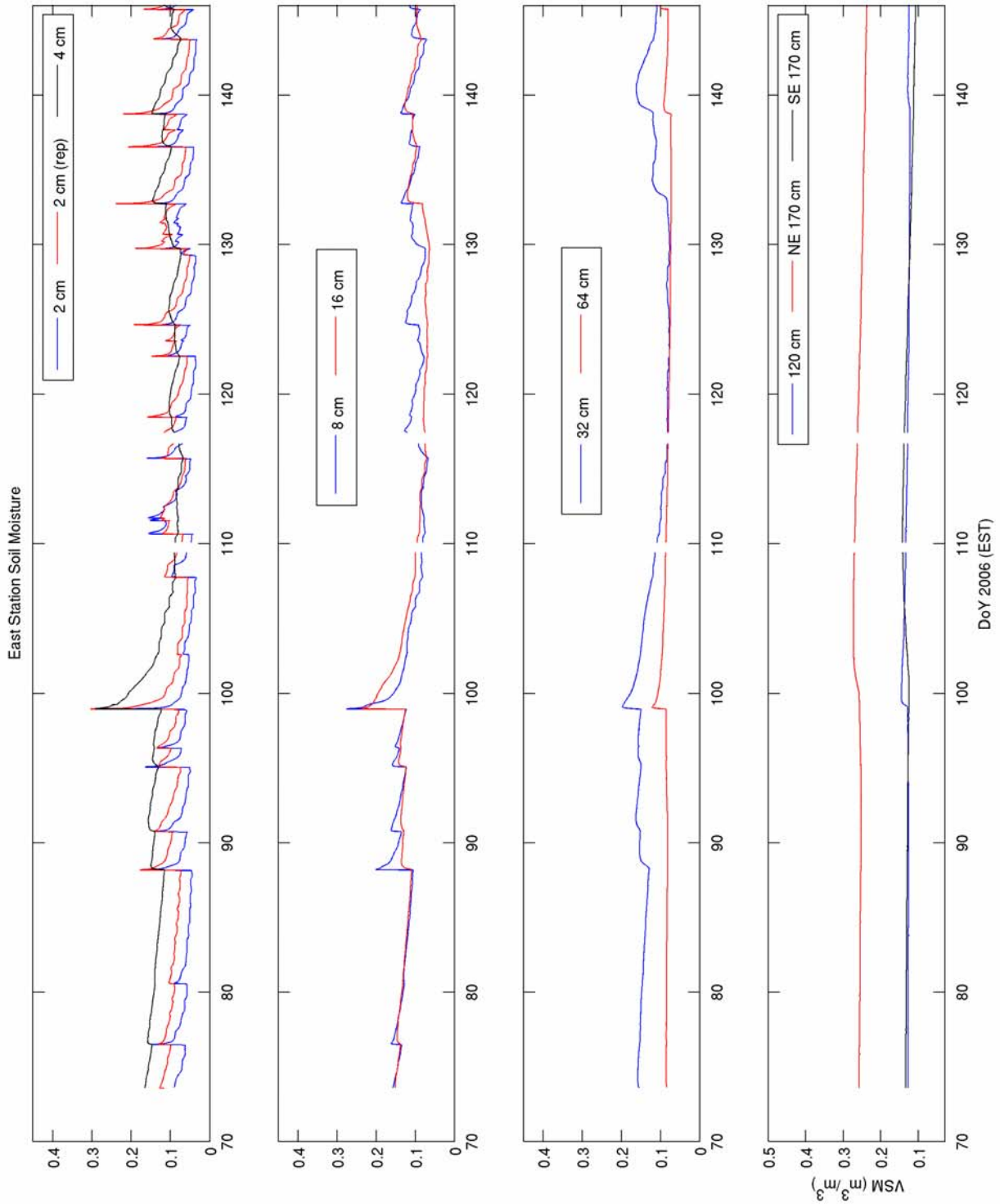

Figure A- 15 East station soil moisture

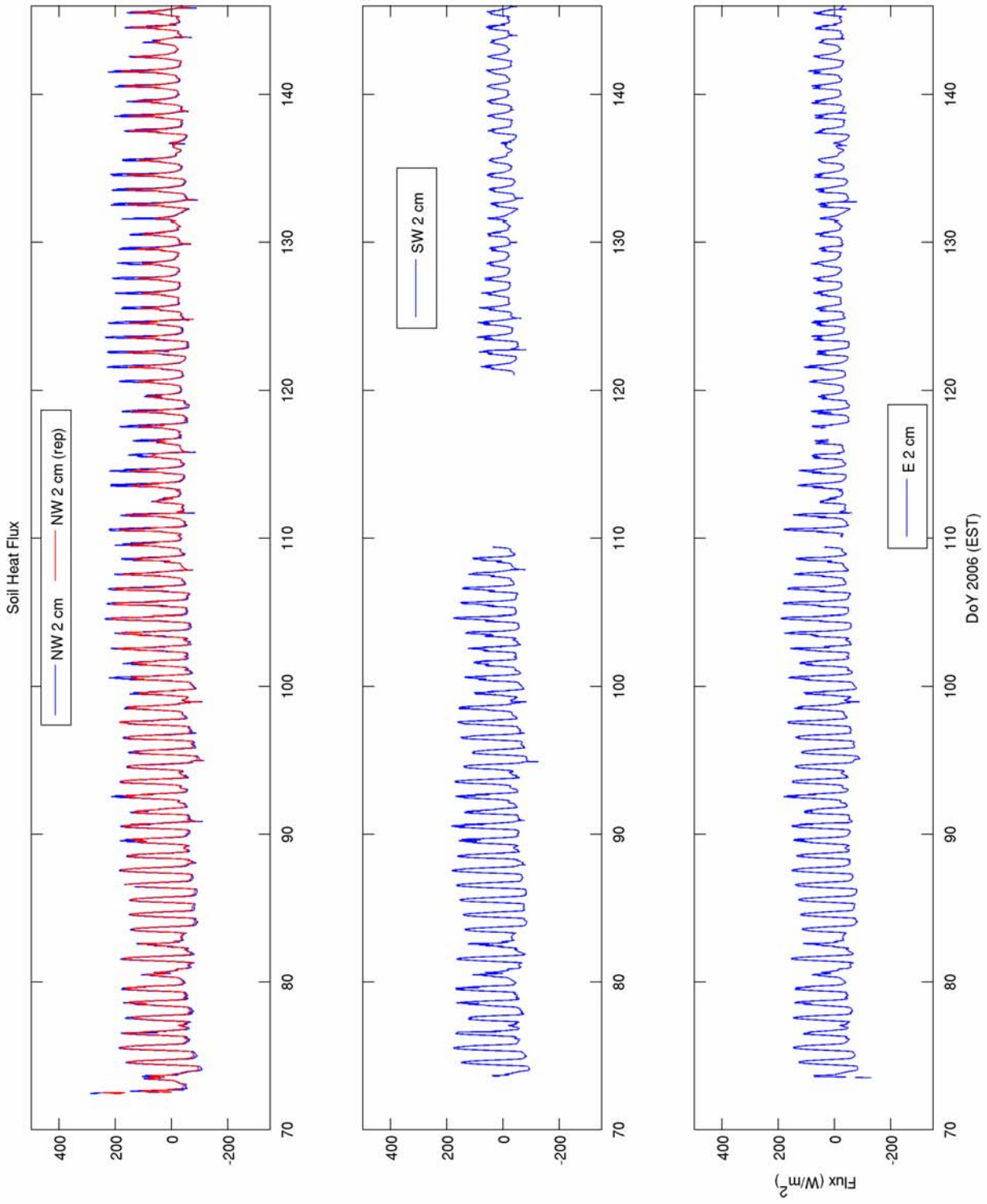

Figure A- 16 Northwest, East, and Southwest station soil heat fluxes

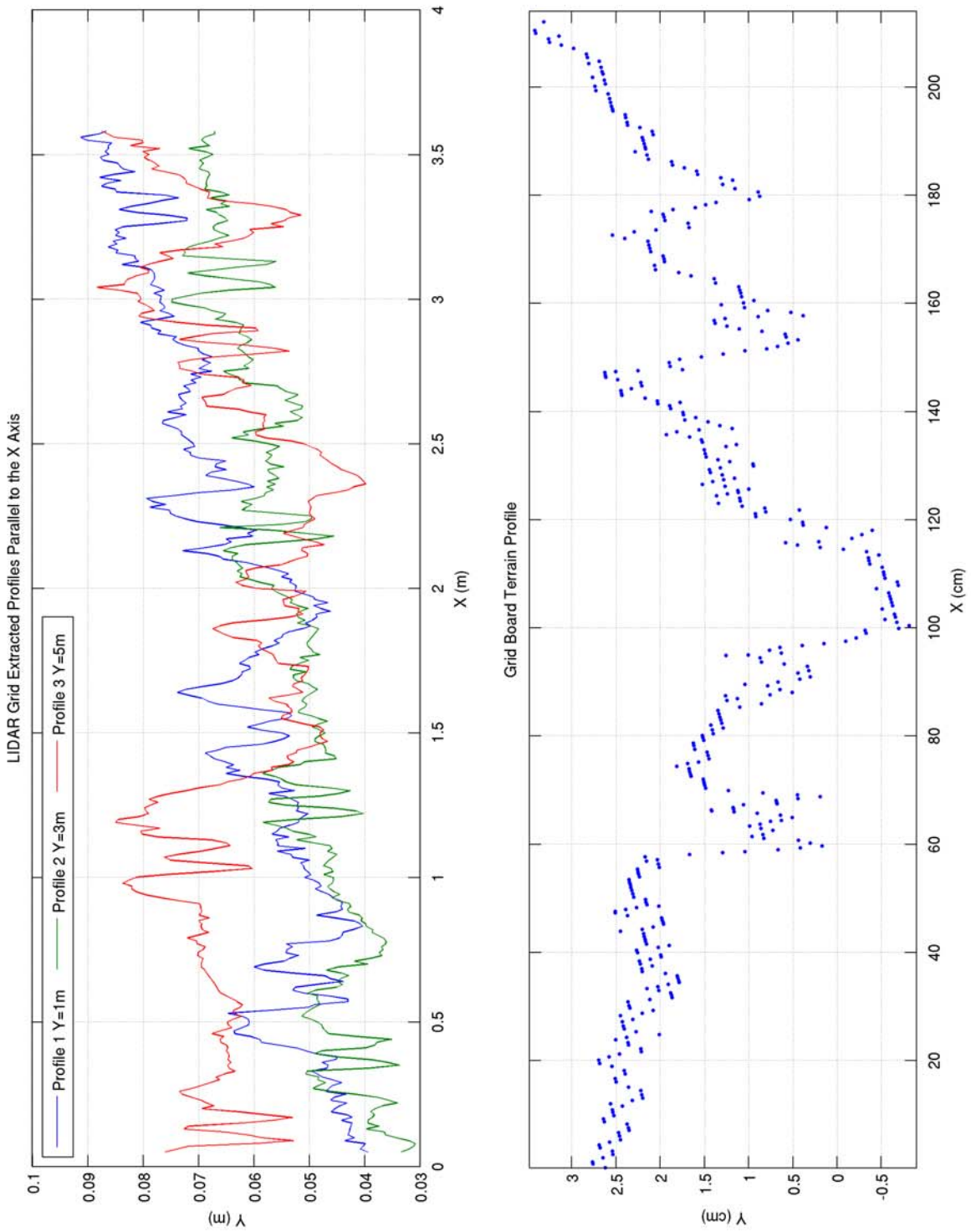

Figure A- 17 Soil roughness profiles, DoY 69

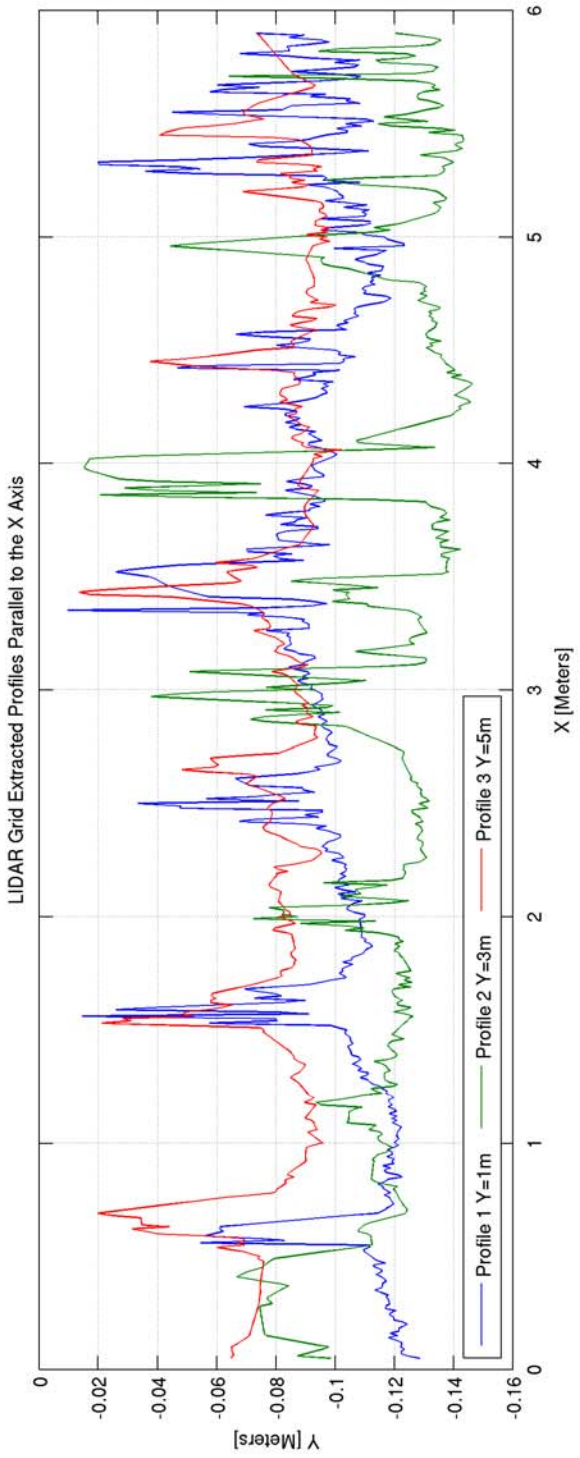

Figure A- 18 Soil roughness profiles, DoY 150

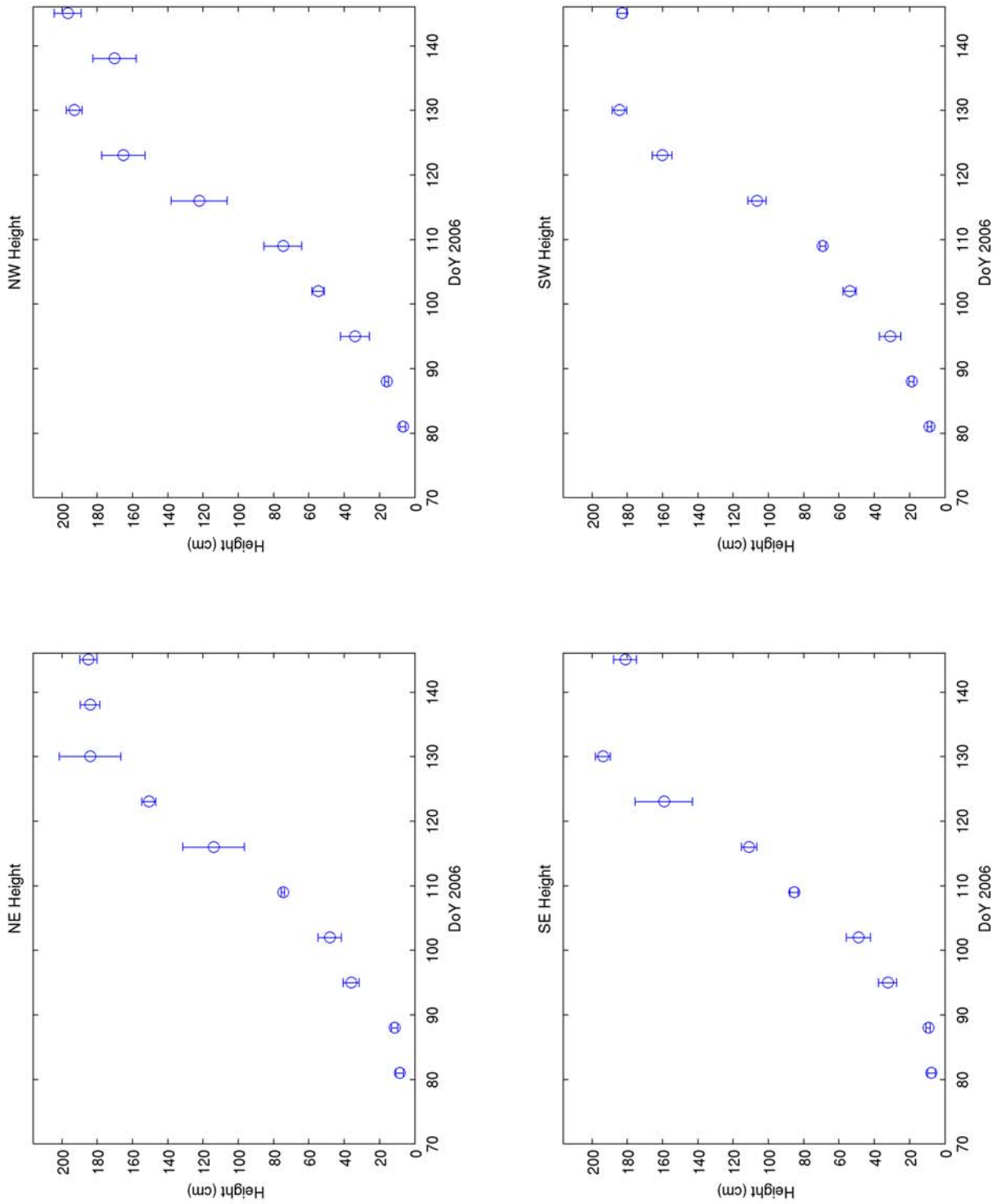

Figure A- 19 Canopy height

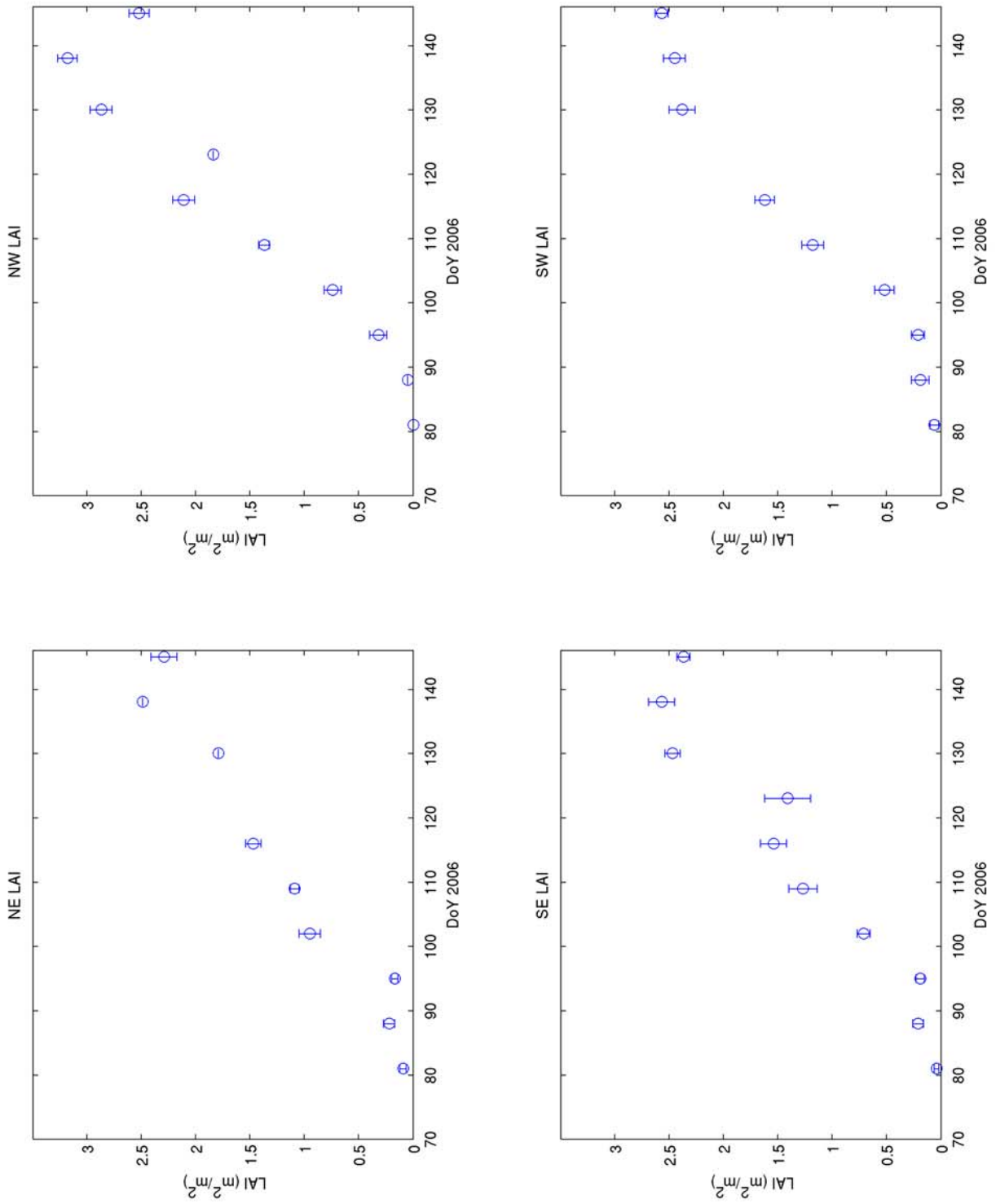

Figure A- 20 Canopy LAI

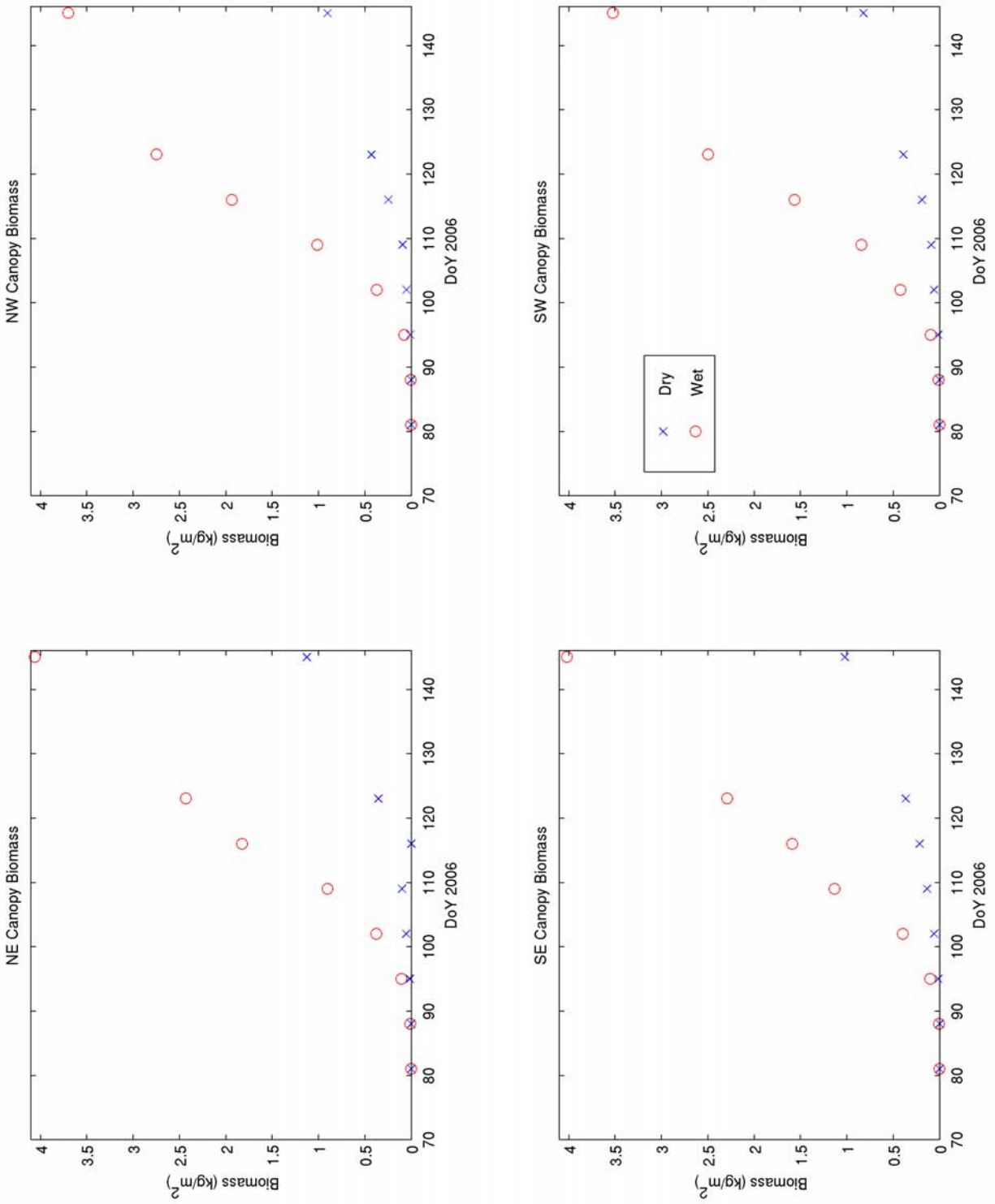

Figure A- 21 Green and Dry canopy biomass

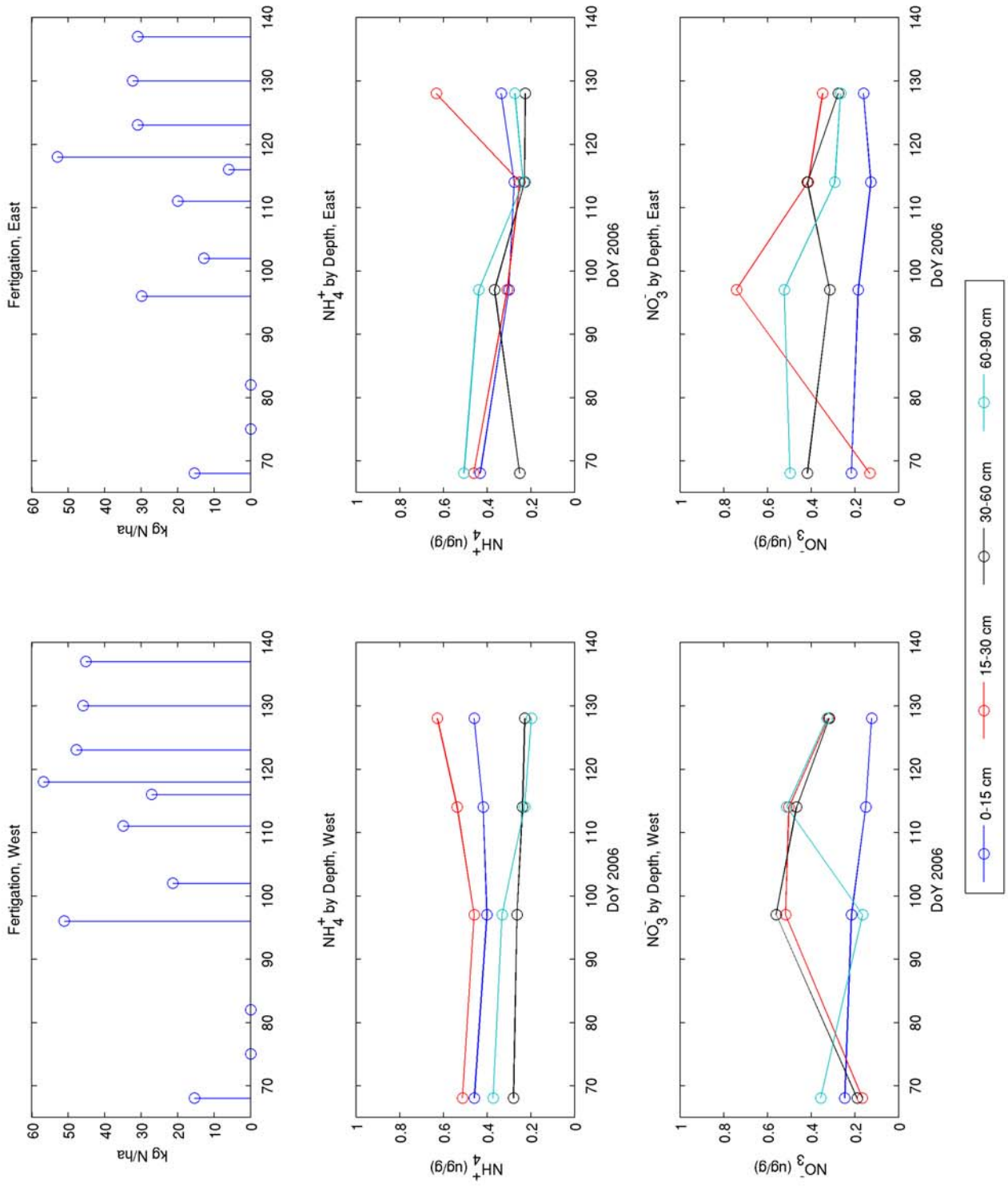

Figure A- 22 Nitrogen sampling

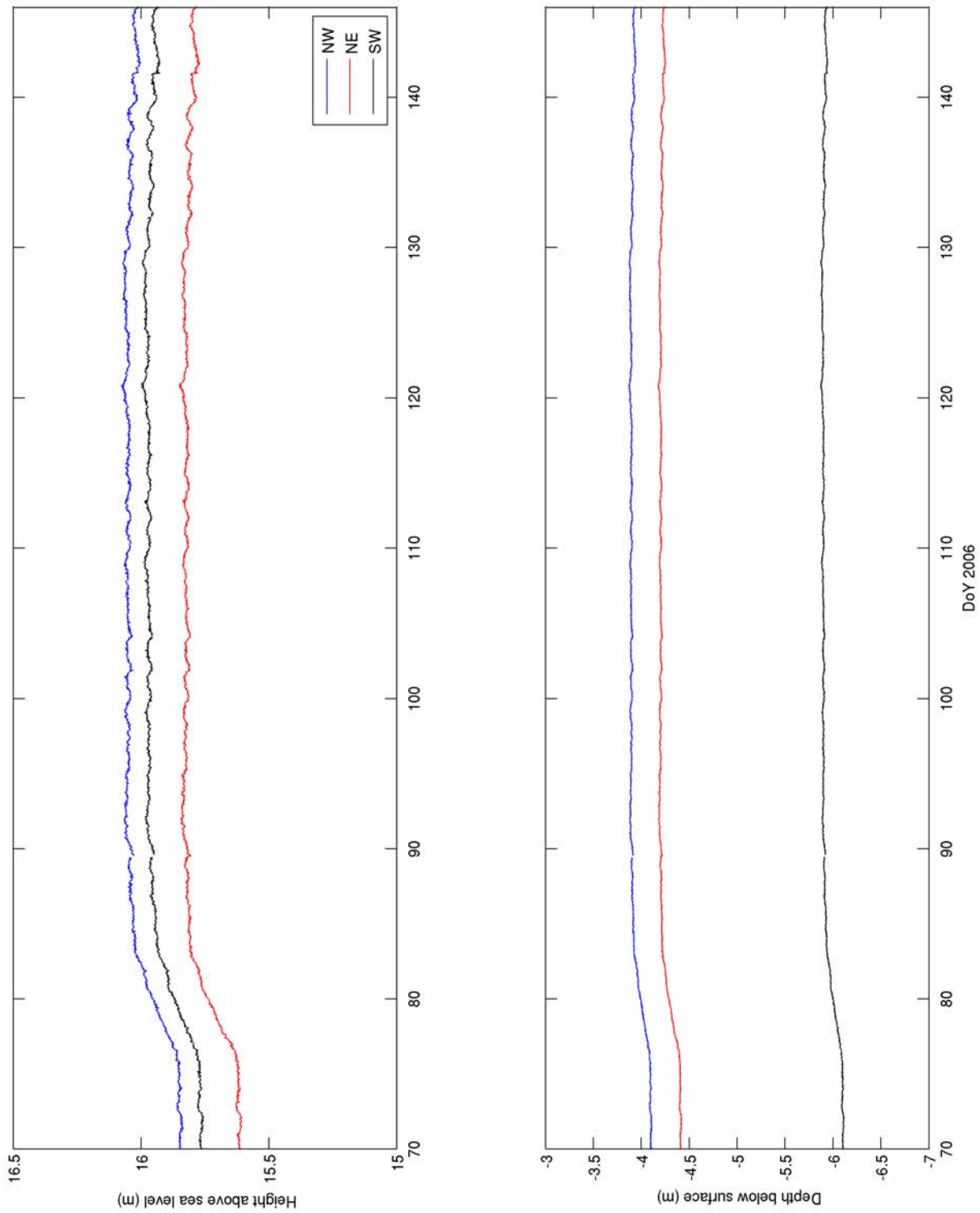

Figure A- 23 Water table depth and elevation above sea level